



Improved Time-Varying Tooth Stiffness Calculation in Cracked Spur Gear Using Modified Limiting Line

Satyajit Mahapatra¹ · Amiya Ranjan Mohanty¹

Received: 14 October 2023 / Revised: 1 March 2024 / Accepted: 19 March 2024
© Springer Nature Singapore Pte Ltd. 2024

Abstract

Purpose Defects and cyclic loads often lead to tooth-root cracks in spur gear transmission systems, affecting system stiffness, vibration patterns, and lifespan. Traditional methods using straight limiting lines and parabolic curves to assess reduced load-bearing areas due to cracks have limitations, including substantial errors with deep cracks and incompatibility with semi-analytical techniques.

Methods This paper introduces a novel approach: a modified limiting line for calculating gear mesh stiffness over a broader range of crack depths. Gear body is treated as rigid to avoid error in gear-body deflection estimates. The modified limiting line is defined by minimizing the difference between mesh stiffness obtained using analytical and finite element methods at a particular mesh position. Moreover, the orientation is used to derive mesh stiffness at additional mesh sites for a given crack configuration. Also, an optimization problem involving a compatibility condition is proposed to determine the load-sharing ratios during double tooth pair engagement.

Results The optimization problems, featuring nonlinear constraints, are solved using sequential quadratic programming. The mesh stiffness and load-sharing ratios are obtained for various crack configurations and are verified using the finite element method. Moreover, the dynamic responses at different crack levels are obtained.

Conclusions The current approach demonstrates better accuracy at higher crack levels than the existing analytical methods and is computationally less expensive than finite element methods.

Keywords Gear mesh stiffness · Limiting line · Tooth root crack · FEM · Load sharing ratio

Introduction

To avoid catastrophic gear failures and for vibration-based condition monitoring, it is of utmost significance to model the gear drive system precisely. The time-varying mesh stiffness computation has drawn considerable attention to enhance the gear drive model. Several calculation efforts have been made to investigate the mesh stiffness of spur gear pairs, including experimental, finite element (FE) and analytical methods. Yesilyurt et al. [1] used modal experimental modal analysis to compute the reduction in gear tooth stiffness due to wearing. Munro et al. [2] proposed a method based on Harris maps to obtain stiffness of spur gear pair experimentally. They included extended contact region when

cornering contact occurs. An experimental methodology [3] based on photo-elasticity technique was presented for obtaining stress intensity factor which was related to variation of effective mesh stiffness in cracked spur gear tooth for single tooth pair contact. Raghuwanshi et al. [4] extended the work for full mesh cycle during double tooth pair contact. Later, the same author [5] utilized strain gauge technique to determine the mesh stiffness for cracked spur gear. Mahapatra et al. [6] estimated the input torque in a two-stage gearbox by measuring the torsional vibrations. Experimental methods [7] are accurate and reliable. However, they necessitate specialized methodologies and sophisticated equipments.

FE methods [8] are also accurate and often require specialized capabilities as mesh stiffness fluctuates over time. Cooley et al. [9] obtained gear mesh stiffness using the average slope and local slope methods. Arafa et al. [8] performed 2d FE analysis using the commercial package COSMOS/M to obtain mesh stiffness. Single-toothed gear-pinion system was modeled, where the pinion was kept fixed at its bore,

✉ Satyajit Mahapatra
smahapatra@iitkgp.ac.in

¹ Department of Mechanical Engineering, Indian Institute of Technology, Kharagpur 721302, India

and the wheel was applied a torque by loading two equal and opposite tangential loads at its bore. Liang et al. [10] obtain the linear mesh stiffness from torsional mesh stiffness by obtaining the angular deflections at the gear end. One of the key for accurate FE modelling is the element size [7]. Contact regions should contain high-density mesh [11] with controlled transition to larger elements at other locations. FE methods are computationally expensive.

Due to the computational challenges, mesh stiffness is often calculated using analytical methods. In 1980, Yang and Lin [12] considered the gear tooth as a non-uniform cantilever beam and established the analytical potential energy method by assuming that the total energy stored in a gear tooth is sum of bending energy, axial compression energy and Hertzian contact energy. Tian [13] later introduced the shearing energy into consideration. The above works did not consider the gear body flexibility, and the TVMS was overestimated. Chen and Shao [14] improved the calculation of TVMS by incorporating the gear body deflection derived by Sainsot et al. [15] using Mushkelliville's circular ring theory [16]. The work was limited to single tooth pair engagement. Later, Xie et al. [17] adopted quadratic and cubic stress distributions along the tooth and gear-body junction to derive analytical formulas to calculate the fillet foundation deflections considering the structural coupling effect. Many researchers [18, 19] proposed different semi-analytical models to deal with the deficiency of an analytical formula for gear body stiffness when double tooth pair contact occurs. Ma et al. utilized correction factors [19] calculated in conjunction with FE method to calculate the gear body flexibility. Based on contact mechanics, Dai et al. [20] proposed an improved mathematical model to obtain gear mesh stiffness. Due to cornering contact, extended tooth contact can occur under larger torques. Ma et al. [21] obtained mesh stiffness considering extended tooth contact. Methods for calculating mesh stiffness for healthy gears have evolved over time. Nevertheless, the computation of mesh stiffness for defective gears is being presented below.

Due to fatigue or high service load, a crack might develop at a high-stress concentration location [22]. Lewick et al. [23] studied the influence of the gear body thickness on the direction of crack propagation. The backup ratio, defined as the ratio of gear-body thickness to tooth height, affects the crack propagation direction. It was established that a lower backup ratio would cause the crack to propagate through the gear body. However, the crack may propagate through the gear body with a lower initial angle, even if with a higher backup ratio. Later, the same author [24], using the principles of linear elastic fracture mechanics estimated the stress intensity factors to model the crack propagation directions. Extended finite element method is beneficial for mesh stiffness determination [25] for discontinuity due to faults like cracks.

In their crack model, Zouari et al. [26] examined the effects of the crack position, direction, and depth on the mesh stiffness and transmission error. By improving the model suggested by Yang and Lin [12] and examining the impact of the crack propagation size on the mesh stiffness, Tian [13] provided an analytical method for modeling the crack for mesh stiffness evaluation by defining a straight limiting line that designates an unloaded load-bearing zone known as the dead zone. Wu et al. [27] obtained the mesh stiffness of spur gear analytically under various tooth root crack levels, assuming straight line path for crack propagation direction. They modeled the gear-rotor system with a lumped parameter scheme and obtained the dynamic responses to be analyzed. They studied the influence of crack on various statistical indicators. Later, three different crack propagation scenarios were investigated by Mohammed et al. [28]. Firstly, they assumed the crack propagation path to be straight and uniform across the width. In the second case, the crack path was considered parabolic, and lastly, they assumed the crack path in both depth and width direction. Chaari et al. [29] examined the stiffness reduction phenomena in spur gear transmission by accounting for two forms of tooth faults: tooth breaking and spalling. Ma et al. [19] established a revised model to predict the mesh stiffness of spur gear with a tooth root crack while accounting for a more realistic tooth root transition curve. Zhou et al. [30] established a mathematical model by considering the gear body as a semi-planar cantilever beam and derived the formula for gear meshing stiffness with different crack levels. An analytical model was put forth by Chen and Shao [31] to determine the mesh stiffness of gears with cracks propagating along both tooth width and depth directions. The determination of gear body flexibility has been a challenging task for a cracked gear. Yang et al. [32] proposed that the root position of cracked tooth should be redefined using the connecting line between the crack root and the endpoint of transition curve. More recently, researchers conducted studies on mesh stiffness for high contact ratio gears, which are smoother compared to low contact ratio gears. Huang et al. [33] established a dynamic model for high contact ratio gears (HCR) with multiple clearances. Later, Nandu et al. [34] conducted a parametric study of the fracture properties of a non-standard HCR spur gear. Mohammed et al. [35] extended the analysis of HCR gears to the modification of gear tooth addendum dimensions for obtaining a high contact ratio for incipient fault detection. The dynamic responses of the gear-rotor system were obtained, and various time domain indicators were analyzed for different crack scenarios.

In most of the above works, crack is modeled by consideration of a straight limiting line that designates an altered load-bearing zone. Mohammed et al. [36] reported that using the traditional straight limiting line induces error at higher

crack levels. To overcome this, they proposed the parabolic limiting curve based on variation in stress gradient which is difficult to identify. Cui et al. [37] utilized the concept of a parabolic curve as the limiting line for mesh stiffness evaluation, considering the universal equation of gear profile. Results were compared using the traditional straight limiting line and the parabolic curve method, establishing that the latter method showed better accuracy. Recently, Liu et al. [38] used the parabolic limiting curve for mesh stiffness evaluation in spur gear for higher crack levels considering elastoplastic deflection in gears. More recently, Yang et al. [39] studied two crack types, tooth root crack and surface crack and utilized the straight limiting line to model the cracks and were able to show that the traditional limiting line showed accurate results even at higher crack depths. The results shown in the above few works seem contradictory. In all of these above works, the gear body flexibility is determined either using the method of correction factor [19] or the gear body deflection equations containing the curve fitting constants proposed by Xie et al. [17] for healthy gears. The calculation errors for gear body deflections for three healthy gear pairs used [17] vary from 7.19 to 28.56%, and for structural coupling-induced tooth deflections, the error varies from 0.55 to 5.23%. So, we believe that the effect of the limiting line used on the tooth stiffness calculation alone has not been given priority. The error in gear-body calculations is one of the reasons for the contradicting results. Any error in the gear-body calculation formula will misinterpret the use of a correct limiting line. So, it is important to establish a standard limiting line considering the tooth stiffness alone that can be more generally useful. Hence, the gear body is assumed to be rigid in this study. A straight limiting line has been shown to produce large errors at higher crack levels [36]. The parabolic curve established in ref³⁶ follows the variation of stress gradients and is difficult to be identified distinctively. Also, the parabolic curve presented by Liu et al. [37, 38] is unique with respect to crack tip and tooth vertex due to the nature of curve equation proposed. This is also discussed in more detail in "[Parabolic Limiting Line](#)". Therefore, for different crack path configurations with same crack tip, it cannot calculate the mesh stiffness accurately. Therefore, a modified limiting line that connects the crack tip but is not constrained to the tooth vertex and is more suitable to be used in conjunction with FE method is established here. To embolden the relevance of the novel approach, the results of an illustrative cantilever beam are compared with the existing methods. Later, the proposed scheme is applied to time-varying tooth stiffness calculation for spur gear under various crack configurations. A minimization problem with nonlinear constraints is formulated by acquiring the mesh stiffness using the FE method.

Further, the sequential quadratic programming (SQP) [40] algorithm is implemented to solve for the obliquity of the limiting line. The proposed method requires FE simulation at a particular gear meshing position during single tooth pair contact to determine the orientation of the modified limiting line. Later, the same orientation can be utilized to obtain tooth stiffness at other mesh positions for a particular crack configuration. Also, an improved load-sharing calculation approach is proposed for tooth stiffness calculation during double tooth pair meshing.

To generate the dynamic responses of the system, the estimated time-varying tooth stiffness is introduced to the dynamic model. The results are analyzed in both frequency and time domain. Further, statistical indicators are used to quantify the crack characteristics. The structure of the paper is as follows:

"[Traditional Time-Varying Tooth Stiffness Model for Cracked Tooth](#)" describes the existing tooth stiffness models for cracked teeth of spur gear. The modified limiting line and, subsequently, the proposed model for tooth stiffness calculation is developed in "[Proposed Tooth Stiffness Model for Cracked Case](#)". The FE modeling for time-varying stiffness evaluation is explained in "[Finite Element Method for Tooth Stiffness Evaluation](#)". "[Results and Discussion](#)" presents the results and discussion.

Traditional Time-Varying Tooth Stiffness Model for Cracked Tooth

The existing analytical method for mesh stiffness evaluation requires that the gear tooth be treated as a cantilever beam with a continuously varying cross-section. Due to the emergence of a crack, the cross-sectional area and moment of inertia of a defective gear tooth are reduced. Here, the potential energy method [13] is employed to determine the tooth stiffness of healthy teeth. It is assumed that the gear is static, and the contact force traverses the involute profile of the non-uniform cantilever beam being fixed at the base circle. We take into account the more realistic scenario when the tooth is fixed on the dedendum circle. As depicted in Fig. 1, the tooth profile is composed of three distinct curves: the involute curve CD, the straight line BC, and the circular fillet curve AB. Potential energy owing to bending, shearing, and axial compression generated by force F at a distance x from D is provided by Eqs. (1), (2), and (3), respectively [13]. F is resolved into transverse and axial directions as F_t and F_a , respectively. x , d and L are defined in Fig. 1. d_1 and d_2 are distances from Y-axis in the opposing directions from C to B and B to A. α_1 is the pressure angle.

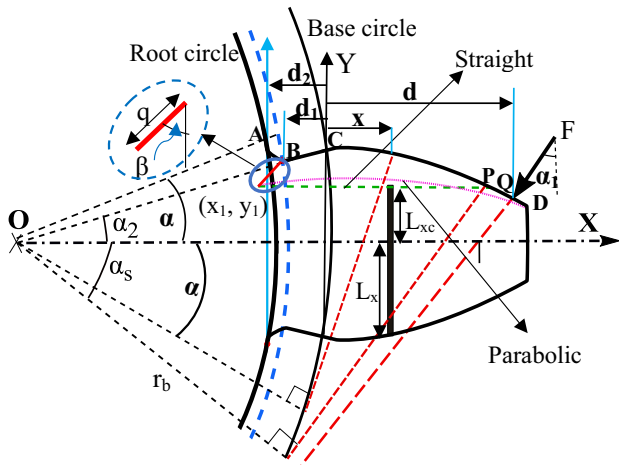


Fig. 1 Geometric parameters of cracked spur gear

$$U_b = \frac{F^2}{2k_b} = \int_0^d \frac{[F_t(d-x) - F_a L]^2}{2EI_x} dx + \int_0^{d_1} \frac{[F_t(d+x) - F_a L]^2}{2EI_x} dx + \int_{d_1}^{d_2} \frac{[F_t(d+x) - F_a L]^2}{2EI_x} dx \quad (1)$$

$$U_s = \frac{F^2}{2k_s} = \int_0^d \frac{1.2F_t^2}{2GA_x} dx + \int_0^{d_1} \frac{1.2F_t^2}{2GA_x} dx + \int_{d_1}^{d_2} \frac{1.2F_t^2}{2GA_x} dx \quad (2)$$

$$U_a = \frac{F^2}{2k_a} = \int_0^d \frac{F_a^2}{2EA_x} dx + \int_0^{d_1} \frac{F_a^2}{2EA_x} dx + \int_{d_1}^{d_2} \frac{F_a^2}{2EA_x} dx \quad (3)$$

where k_b , k_s and k_a are gear tooth stiffness due to bending, shearing and axial compression, respectively. E and G are the modulus of elasticity and rigidity of the gear material, respectively. In the traditional approach [9], the Hertzian contact stiffness was independent of the contact force. Here, load-dependent Hertzian contact stiffness [17, 38] is used (Eq. (4)). W is the gear face width. Hertzian contact stiffness [17] (k_h) is given by

$$k_h = \frac{E^{0.9} W^{0.8} F^{0.1}}{1.275} \quad (4)$$

The area moment of inertia I_x and area of cross-section A_x in Eqs. (1), (2) and (3) are defined as follows:

For healthy gear,

$$I_x = \frac{8WL_x^3}{3}, A_x = 2WL_x, \text{ where, } L_x = \begin{cases} r_b((\alpha_2 + \alpha) \cos \alpha - \sin \alpha) & \text{for } 0 \leq x \leq d'' \\ r_b \sin \alpha_2 - x \tan \alpha_2 & \text{for } 0 < x < d_1'' \\ y_c - \sqrt{r_f^2 - (x - x_c)^2} & \text{for } d_1 \leq x \leq d_2'' \end{cases} \quad (5)$$

r_b and r_d are base circle and addendum circle radii. r_f is the fillet radius. Half tooth angle $\alpha_2 = \frac{\pi}{2N} + \tan \alpha_0 - \alpha_0$, N is the number of teeth, and α_0 is the pressure angle. The center coordinates (x_c and y_c) of the fillet circular arc (portion B to A in Fig. 1) are obtained from geometry as: $x_c = r_b \cos \alpha_2 - (r_d + r_f) \cos \alpha_f$, $y_c = r_b \sin \alpha_2 + r_f$. Equivalent tooth stiffness (k_t) can be calculated by taking the stiffness due to pinion and gear in series using the formula [13]:

$$\frac{1}{k_t} = \frac{1}{k_{b,p}} + \frac{1}{k_{s,p}} + \frac{1}{k_{a,p}} + \frac{1}{k_h} + \frac{1}{k_{b,g}} + \frac{1}{k_{s,g}} + \frac{1}{k_{a,g}} \quad (6)$$

The subscripts p and g , respectively, denote pinion and gear. Due to the appearance of a crack, the drop in tooth stiffness is caused by a change in geometric parameters I_x and A_x in Eqs. (1) to (6). Identifying the altered load-bearing zone due to the crack yields the geometric parameters. The straight and parabolic limiting lines are utilized for the aforementioned purpose, which is discussed in "Straight Limiting Line" and "Parabolic Limiting Line" below.

Straight Limiting Line

Researchers [12, 13, 27] used the conventional limiting line (the green dashed line depicted as traditional in Fig. 1) to recognize an unloaded zone, also known as a dead zone, caused by a crack. The new load-bearing zone now influences the tooth stiffness calculation by affecting I_x and A_x (Eq. (5)) for the bending and shearing phenomenon. However, the axial compression energy [13] is not impacted.

For cracked gear [27],

$$I'_x = \frac{W(L_x + L_{xc})^3}{12}, A'_x = W(L_x + L_{xc}) \quad (7)$$

where L_x is given by Eq. (5) and $L_{xc} = r_b \sin \alpha_2 - q \cos \beta$, here, q is the crack length, and β is the crack orientation (Fig. 1). α_2 is the half-tooth angle. The different crack cases can be found in Tian's work [13].

Parabolic Limiting Line

The parabolic limiting line originally proposed by Mohammed et al. [36] was utilized by Cui et al. [37] and Liu et al. [38]. It is assumed that the curve connects the tooth addendum vertex and crack tip (point D), as shown in Fig. 1. The parabolic curve equation [38] is given by

$$L_{xc} = \frac{(y_D - y_1)}{(x_D - x_1)^2} (x - x_1)^2 + y_1 \tag{8}$$

Here x_D, y_D are coordinates of point D and x_1, y_1 are the coordinates of the crack tip and are obtained from the geometry. Equation (8) is used in Eq. (7) to obtain the geometric parameters to model the crack for further evaluation of time-varying tooth stiffness using Eqs. (1) to (6). On simplifications, Eq. (8) can be re-written in the form $L_{xc} = ax^2 + bx + c$.

Where, $a = \frac{y_D - y_1}{(x_D - x_1)^2}$, $b = -2x_1 \frac{y_D - y_1}{(x_D - x_1)^2}$ and $c = \frac{y_D - y_1}{(x_D - x_1)^2} x_1^2 + y_1$.

The constants a, b and c are functions of the coordinates of tooth vertex and crack tip and tooth vertex being always fixed. Therefore, the parabolic curve given in Eq. (8) represents a unique curve with respect to the crack tip. Mohammed et al.'s [36] proposed method requires the parabolic curve to be fitted with the finite element results. As a, b and c have constant values, Eq. (8) is not appropriate to be used in the semi-analytical method. Hence, it is necessary to establish a modified limiting line that is not unique and allow it to be fitted with FE results, and that will be an appropriate candidate for mesh stiffness evaluation under the crack. The novel limiting line will be developed in the subsequent sections.

Proposed Tooth Stiffness Model for Cracked Case

The mesh stiffness of a gear is the effective stiffness resulting from tooth and gear body flexibility. Separate calculations have been proposed for gear-body deflections and tooth deflections, and the load sharing connects the calculation methods. So, improving the tooth stiffness calculation method will improve the overall mesh stiffness. The tooth stiffness of spur gears is calculated by considering the tooth as a non-uniform cantilever beam. A fault such as a crack modifies the load-bearing zone and is determined by the effective section width. As the crack parameters affect the effective section width, the cross-sectional area and moment of inertia will likewise change proportionally. The effective section width is calculated based on approaches discussed in "Straight Limiting Line" and "Parabolic Limiting Line" with a straight affecting line and a parabolic affecting curve, respectively. Since straight affecting line produces large error with higher crack levels, it is not suitable for mesh stiffness determination. On the other hand, the parabolic curve, which is fixed on the tooth vertex, is not convenient due to reasons explained in "Parabolic Limiting Line". The present study uses the tooth as a cantilever beam. Hence,

to establish the unloaded zone, first, an illustrative simple cantilever beam with a growing vertical crack (Figure 23 in appendix A) subjected to a concentrated load at its free end is considered to embolden our conviction to establish a modified limiting line in gear. For the sake of brevity, we keep the details in Appendix A, and only the results obtained for cantilever beam are shown here in Fig. 2. Figure 2a displays the comparison of stiffness of cantilever beam using the straight and modified (oblique) limiting line with the FE method.

Figure 2b shows that the percentage error is higher with increasing crack depth for the straight limiting line, whereas for the oblique limiting line considered, the percentage error is close to zero. The orientation of limiting line versus crack length is depicted in Fig. 2c. A similar oblique limiting line can now be established to improve the calculation of tooth stiffness of meshed gears.

Figure 3 depicts the modified limiting line (MLL) forming an angle of θ with the horizontal axis (OX). The solid red line represents the crack with length q , and the crack angle is β with respect to the vertical Y-axis. Figure 3a shows the limiting line crossing the involute profile at a point P between tooth vertex D and point C and satisfies the relation $L_{xc} \geq L_h$ and $\alpha \leq \alpha_s$ from P to D and $\alpha > \alpha_s$ from P to C. Figure 3b displays the limiting line that meets the extended tooth profile and $L_{xc} < L_h$ and $\alpha \leq \alpha_s$ during the whole tooth engagement duration. The moment of inertia (I_x') and area of cross-section (A_x'), along with the reduced section width, are given in Eqs. (9) and (10), respectively.

$$I_x' = \frac{W(L_x + L_{xc})^3}{12}, A_x' = W(L_x + L_{xc}) \tag{9}$$

Section width, L_x for healthy gear is given in Eq. (5) and L_{xc} for the crack case for the proposed scheme is expressed in Eq. (10) below.

$$L_{xc} = \left\{ \begin{array}{l} \tan \theta \times [r_b(\cos \alpha - (\alpha_2 - \alpha) \sin \alpha - \cos \alpha_2) \\ - ((r_d + r_f - r_b) \cos \alpha_2 + q \cos \mu)] \\ + (r_d + r_f) \sin \alpha_2 - q \sin \mu \quad \forall 0 \leq x \leq d \\ \tan \theta \times [-x - ((r_d + r_f - r_b) \cos \alpha_2 + q \cos \mu)] \\ + (r_d + r_f) \sin \alpha_2 - q \sin \mu \quad \forall 0 \leq x \leq d_1 \\ \tan \theta \times [-x - ((r_d + r_f - r_b) \cos \alpha_2 + q \cos \mu)] \\ + (r_d + r_f) \sin \alpha_2 - q \sin \mu \quad \forall d_1 \leq x \leq d_2 \end{array} \right\} \tag{10}$$

The bending, shearing, and axial compression stiffness due to the appearance of a crack are derived in Eqs. (10) through (16) below for two cases. Figure 3a depicts a situation when the MLL cuts the involute profile at point P, and for calculation of stiffness is based on case-1 (Eqs. (11) to (13)). On the other hand, Fig. 3b shows the condition that

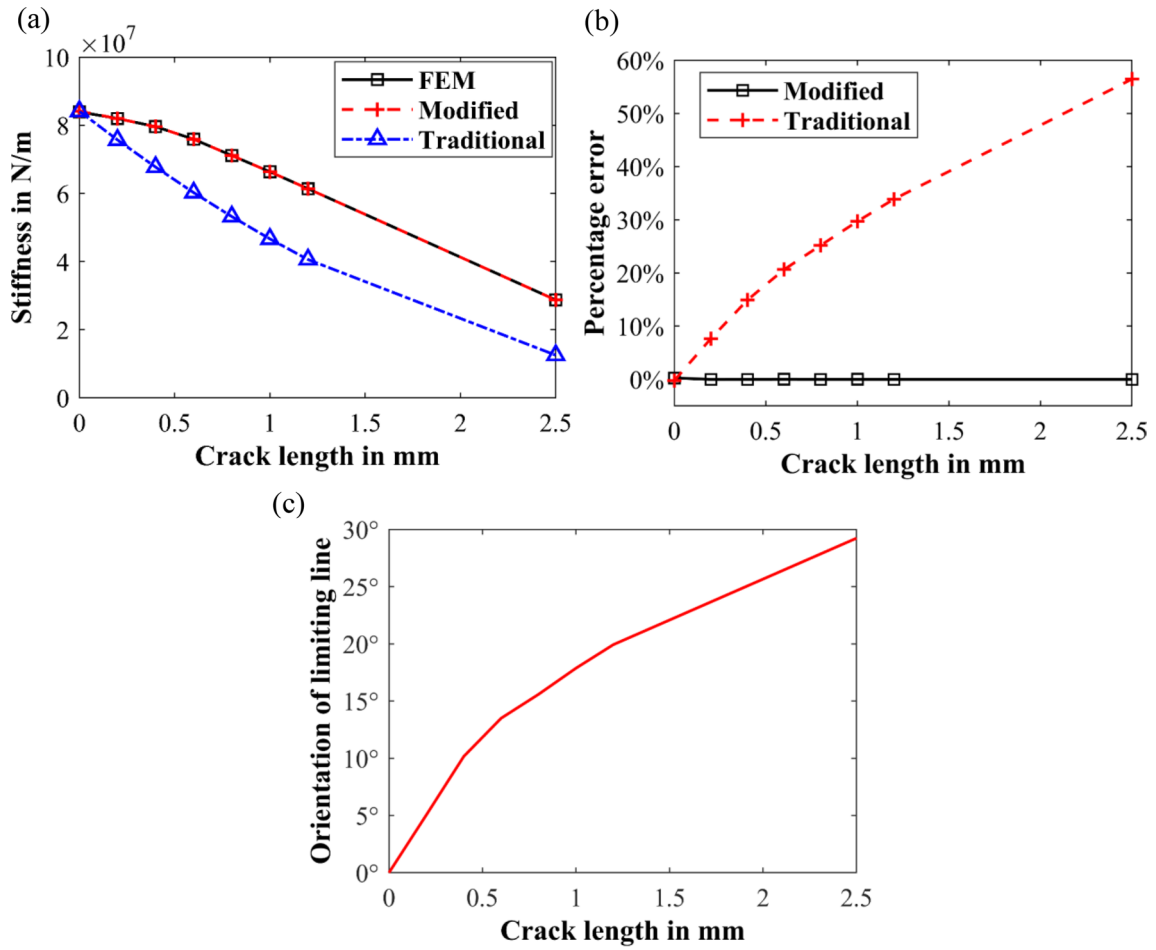
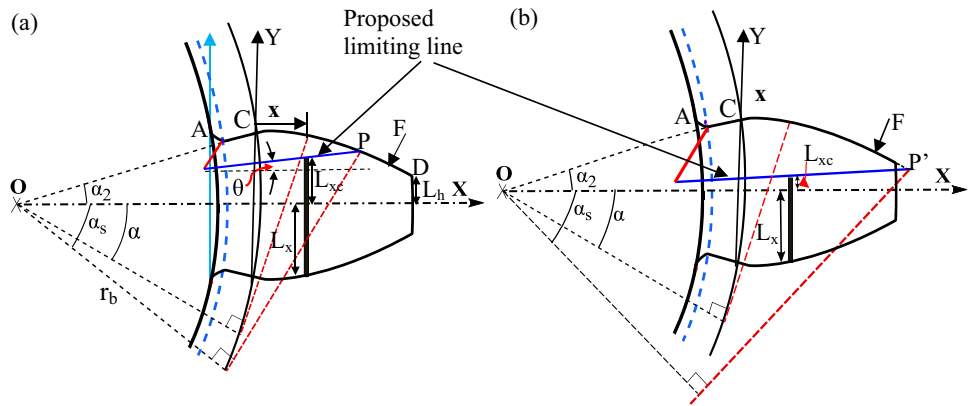


Fig. 2 **a** Comparison of stiffness of cantilever. **b** Percentage error using the proposed method and traditional method for various crack lengths. **c** Orientation of limiting line

Fig. 3 Gear tooth with modified limiting line(MLL) for two different crack cases. **a** MLL cuts the tooth profile. **b** MLL intersects on extended tooth profile



MLL meets on the extension of the involute profile outside the teeth, and the calculation of stiffness is based on equations in case-2 (Eqs. (14) to (16)).

Case (1): $L_{xc} \geq L_h$ and $\alpha > \alpha_s$

$$\begin{aligned} \frac{1}{k_b} = & \int_{-\alpha_1}^{-\alpha_s} \frac{[12(1 + \cos \alpha_1 ((\alpha_2 - \alpha) \sin \alpha - \cos \alpha))]^2 (\alpha_2 - \alpha) \cos \alpha}{EI_x} d\alpha \\ & + \int_{-\alpha_s}^{\alpha_2} \frac{[12(1 + \cos \alpha_1 ((\alpha_2 - \alpha) \sin \alpha - \cos \alpha))]^2 (\alpha_2 - \alpha) \cos \alpha}{EI'_x} d\alpha \\ & + \int_0^{d_1} \frac{12[(r_b - r_b \cos \alpha_1) + x \cos \alpha_1]^2}{EI'_x} dx \\ & + \int_{d_1}^{d_2} \frac{12[(r_b - r_b \cos \alpha_1) + x \cos \alpha_1]^2}{EI'_x} dx \end{aligned} \tag{11}$$

$$\begin{aligned} \frac{1}{k_s} = & \int_{-\alpha_1}^{-\alpha_s} \frac{1.2(\alpha_2 - \alpha) \cos \alpha \cos^2 \alpha_1}{GA_x} d\alpha \\ & + \int_{-\alpha_s}^{\alpha_2} \frac{1.2(\alpha_2 - \alpha) \cos \alpha \cos^2 \alpha_1}{GA'_x} d\alpha \\ & + \int_0^{d_1} \frac{1.2 \cos^2 \alpha_1}{GA'_x} dx + \int_{d_1}^{d_2} \frac{1.2 \cos^2 \alpha_1}{GA'_x} dx \end{aligned} \tag{12}$$

$$\frac{1}{k_a} = \int_{-\alpha_1}^{\alpha_2} \frac{(\alpha_2 - \alpha) \cos \alpha \sin^2 \alpha_1}{2EA_x} d\alpha + \int_0^{d_1} \frac{\sin^2 \alpha_1}{2EA_x} dx + \int_{d_1}^{d_2} \frac{\sin^2 \alpha_1}{2EA_x} dx \tag{13}$$

Case (2): ($L_{xc} < L_h$ or $L_{xc} \geq L_h$) and $\alpha \leq \alpha_s$

$$\begin{aligned} \frac{1}{k_b} = & \int_{-\alpha_1}^{\alpha_2} \frac{[12(1 + \cos \alpha_1 ((\alpha_2 - \alpha) \sin \alpha - \cos \alpha))]^2 (\alpha_2 - \alpha) \cos \alpha}{EI'_x} d\alpha \\ & + \int_0^{d_1} \frac{12[(r_b - r_b \cos \alpha_1) + x \cos \alpha_1]^2}{EI'_x} dx \\ & + \int_{d_1}^{d_2} \frac{12[(r_b - r_b \cos \alpha_1) + x \cos \alpha_1]^2}{EI'_x} dx \end{aligned} \tag{14}$$

$$\begin{aligned} \frac{1}{k_s} = & \int_{-\alpha_1}^{\alpha_2} \frac{1.2(\alpha_2 - \alpha) \cos \alpha \cos^2 \alpha_1}{GA'_x} d\alpha \\ & + \int_0^{d_1} \frac{1.2 \cos^2 \alpha_1}{GA'_x} dx + \int_{d_1}^{d_2} \frac{1.2 \cos^2 \alpha_1}{GA'_x} dx \end{aligned} \tag{15}$$

$$\frac{1}{k_a} = \int_{-\alpha_1}^{\alpha_2} \frac{(\alpha_2 - \alpha) \cos \alpha \sin^2 \alpha_1}{EA_x} d\alpha + \int_0^{d_1} \frac{\sin^2 \alpha_1}{EA_x} dx + \int_{d_1}^{d_2} \frac{\sin^2 \alpha_1}{EA_x} dx \tag{16}$$

The local Hertzian stiffness is calculated using Eq. (4). Equation (6) is further used along with equations in case-1 and case-2 to obtain the effective tooth stiffness.

The above equations are entirely defined for the traditional limiting lines (straight and parabolic). However, the proposed limiting line requires the orientation θ (Fig. 3a) to be determined. In order to obtain the orientation (θ) of the modified limiting line, a minimization problem is formulated, which is described below in "Formulation of Minimization Problem for Determination of Orientation of Modified Limiting Line".

Formulation of Minimization Problem for Determination of Orientation of Modified Limiting Line

The assumption that orientation (θ) of limiting line is independent of the point of action and the force applied ensures that θ depends only on the crack parameters. On the condition that tooth stiffness obtained from finite element analysis at a particular gear contact position is available, the error is the difference between theoretical (k_t) and FE obtained (k_{FEM}) stiffness. In order to constrain the minimum error to a small positive value (near zero), the fitness function is formulated by the square of error (E) (Eq. (17))

$$\begin{aligned} \text{Minimize } f(\theta, \alpha_s) = & E^2 \\ = & (k_{FEM} - k_t)^2, \text{ subject to } 0^\circ \leq \theta \leq 90^\circ \text{ and} \\ & -\alpha_2 \leq \alpha_s \leq \alpha_{\max} \end{aligned} \tag{17}$$

The angle α_s depicted in Fig. 3 is a function of θ , which can be obtained by solving the minimization problem (Eq. (17)). The constraint equation is formed by equating the coordinates of the intersection point of the revised limiting line and the involute tooth curve.

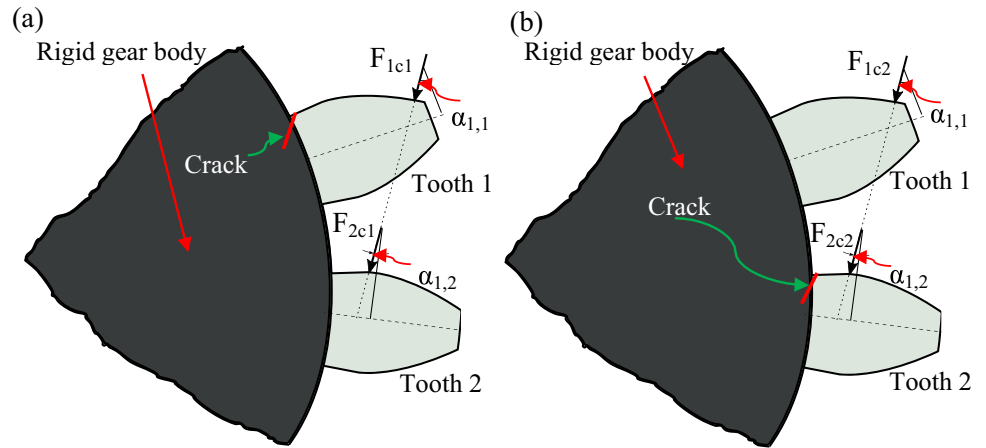
$$\begin{aligned} r_b [(\alpha_2 + \alpha_s) \cos \alpha_s - \sin \alpha_s] - \tan \theta \\ \times [r_b (\cos \alpha - (\alpha_2 - \alpha_s) \sin \alpha_s - \cos \alpha_2)] \\ + \tan \theta \times ((r_d + r_f - r_b) \cos \alpha_2 + q \cos \mu) \\ - (r_d + r_f) \sin \alpha_2 + q \sin \mu = 0 \end{aligned} \tag{18}$$

The above minimization problem with the nonlinear constraint (Eqs. (17) and (18)) can be solved by the method that will be described later in "Sequential Quadratic Programming". Now, as MLL is completely defined, it can be used to obtain the stiffness during double tooth pair meshing.

Tooth Stiffness During Double Tooth Pair Meshing

The contact load is shared between two teeth during double tooth pair meshing, as shown in Fig. 4. If the individual effective stiffness of tooth-1 and tooth-2 are k_1 and k_2 , respectively,

Fig. 4 Load sharing during double tooth pair engagement. **a** Crack in tooth1. **b** Crack in tooth 2



and the corresponding loads shared are F_1 and F_2 , then from energy balance, the equivalent stiffness for the healthy case can be written as:

With $\frac{1}{k_1} = \frac{1}{k_{t1}} + \frac{1}{k_{h1}}$ and $\frac{1}{k_2} = \frac{1}{k_{t2}} + \frac{1}{k_{h2}}$, the effective tooth stiffness [17]

$$k = \frac{k_1 k_2}{k_2 lsr_1^2 + k_1 lsr_2^2} \tag{19}$$

wherein, $lsr_1 = \frac{F_1}{F}$, $lsr_2 = \frac{F_2}{F}$, k_{h1} and k_{h2} are respective Hertzian contact stiffness and k_{t1} and k_{t2} are tooth stiffness of first and second tooth pairs and are given by

$$\frac{1}{k_{t,i}} = \frac{1}{k_{b,p,i}} + \frac{1}{k_{s,p,i}} + \frac{1}{k_{a,p,i}} + \frac{1}{k_{b,g,i}} + \frac{1}{k_{s,g,i}} + \frac{1}{k_{a,g,i}} \tag{20}$$

Here, p and g represent pinion and gear, and $i = 1, 2$ represent the first and second tooth pair, respectively.

Now, for crack case, when the first tooth (Fig. 4a) and subsequently, the second tooth (Fig. 4b) contains the crack, let the stiffness of tooth pair-1 be k_{c1} and tooth pair-2 be k_{c2} respectively, then the equivalent stiffness can be written as [37]:

$$k_c = \left\{ \begin{array}{l} \frac{k_{c1} k_2}{k_2 lsr_{1c1}^2 + k_{c1} lsr_{2c1}^2} \text{ for tooth pair 1 contains the crack} \\ \frac{k_1 k_{c2}}{k_{c2} lsr_{1c2}^2 + k_1 lsr_{2c2}^2} \text{ for tooth pair 2 contains the crack} \end{array} \right\} \tag{21}$$

Here, lsr_{1c1} and lsr_{2c1} are the load-sharing ratios for the case when tooth pair-1 contains the crack and lsr_{1c2} and lsr_{2c2} are load-sharing ratios for the second case when tooth pair-2 has the crack and are related to the shared loads given by equations below:

$$lsr_{1c1} = \frac{F_{1c1}}{F}, \quad lsr_{2c1} = \frac{F_{2c1}}{F}, \quad lsr_{1c2} = \frac{F_{1c2}}{F}, \quad lsr_{2c2} = \frac{F_{2c2}}{F} \tag{22}$$

F_{1c1} , F_{2c1} , F_{1c2} and F_{2c2} are loads shared by tooth-1 and tooth-2 for two cases shown in Fig. 4a, b, respectively. The proposed model for obtaining load-sharing ratios for healthy and two crack cases is explained below.

Most of the previous works use the minimization of potential energy approach proposed by Xie et al. [17] for the determination of load-sharing ratios apart from the correction factor methods. We modify the optimization problem by introducing the compatibility condition. Apart from the potential energy to be minimum for equilibrium, the deflections of the two tooth pairs in contact must be equal without

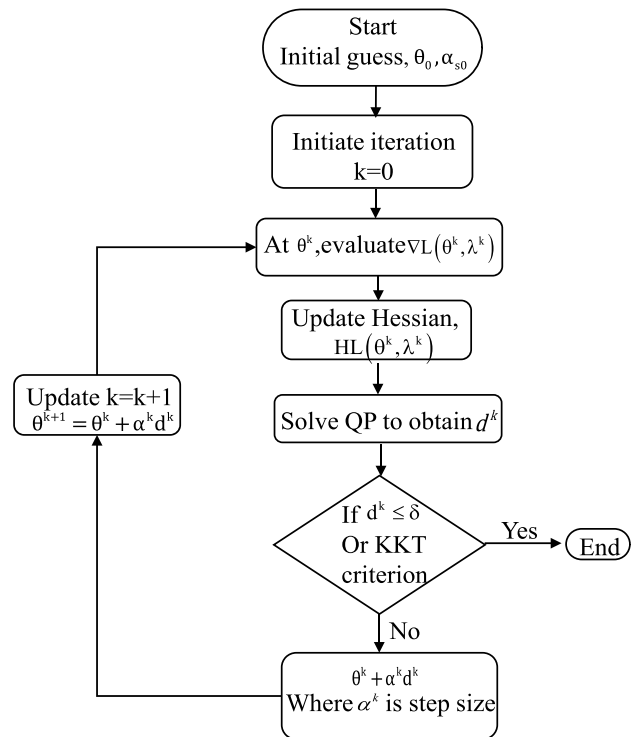
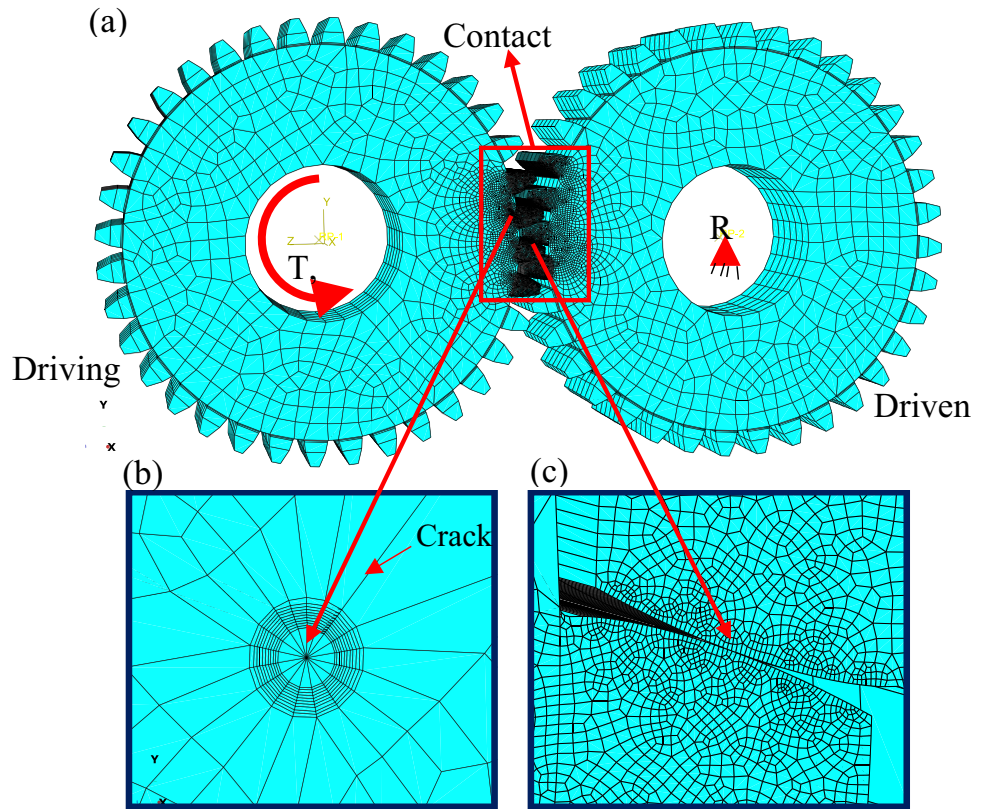


Fig. 5 Sequential quadratic programming algorithm

Fig. 6 3D finite element model of cracked gear. **a** FE meshing of overall gear drive. **b** Wedge elements near crack tip. **c** Smaller elements near tooth contact zone



any transmission error. It results in a nonlinear constrained optimization problem.

Optimization problem:

$$\begin{aligned} \text{Minimize } U &= \frac{F_1^2}{2k_1} + \frac{F_2^2}{2k_2} \text{ subject to } F_1 + F_2 \\ &= F, 0 \leq F_1 \leq F \text{ and } 0 \leq F_2 \leq F \end{aligned} \quad (23)$$

The compatibility condition is obtained by equating the deflections δ_1 and δ_2 of tooth-1 and tooth-2, respectively. Hence, $\delta_2 - \delta_1 = 0$, with $\delta_1 = \delta_{h1} + \delta_{t1}$ and $\delta_2 = \delta_{h2} + \delta_{t2}$, wherein δ_{h1} and δ_{h2} are Hertzian contact deflections and δ_{t1}

and δ_{t2} are tooth deflections of tooth-1 and tooth-2, respectively and are given by Eq. (24).

$$\delta_{h1} = \frac{1.275F_1^{0.9}}{E^{0.9}W^{0.8}}, \delta_{t1} = \frac{F_1}{k_{t1}} \quad \text{and} \quad \delta_{h2} = \frac{1.275F_2^{0.9}}{E^{0.9}W^{0.8}}, \delta_{t2} = \frac{F_2}{k_{t2}} \quad (24)$$

Therefore, the compatibility condition can be written as:

$$\frac{1.275F_2^{0.9}}{E^{0.9}b^{0.8}} + \frac{F_2}{k_{t2}} - \frac{1.275F_1^{0.9}}{E^{0.9}b^{0.8}} - \frac{F_1}{k_{t1}} = 0 \quad (25)$$

The optimization problem can be modified for the crack cases by substituting suitably the tooth stiffness for the first cracked tooth pair as k_{t1c} and the second cracked tooth pair as k_{t2c} in place of k_{t1} and k_{t2} , respectively, in Eqs. (19), (21), (23) and (25). F_1 and F_2 can be appropriately replaced by F_{1c1} , F_{2c1} , F_{1c2} and F_{2c2} . The above optimization problems are solved using the method described below in "Sequential Quadratic Programming".

Sequential Quadratic Programming

In this work, two problems involving minimization with nonlinear constraints have been proposed. One is to obtain the orientation of the proposed limiting line, and the other is to obtain the load-sharing ratios. Xie et al. [17] used the genetic algorithm to solve the linear constraint problem,

Table 1 Gear parameters

	Pinion	Gear
Number of teeth	36	36
Module	1.5	1.5
Pressure angle	20°	20°
Modulus of elasticity	$2.1 \times 10^5 \text{ N/mm}^2$	$2.1 \times 10^5 \text{ N/mm}^2$
Poisson's ratio	0.3	0.3
Fillet radius	0.1 mm	0.1 mm
Hub radius	12 mm	12 mm
Torque	10,000 N mm	10,000 N mm
Gear width	15 mm	15 mm

which is not suitable for the proposed problem here. A more appropriate technique, like a sequential quadratic programming (SQP) algorithm, is adopted here to solve the two optimization problems. Only the procedure for solving the first problem is presented here for the sake of brevity. Necessary parameters can be changed suitably to solve the second problem. The objective of the optimization problem formulated is to find θ, α_s that minimizes $f(\theta, \alpha_s)$ subject to $g(\theta, \alpha_s) = 0$. The Lagrangian function [41] of the problem $L(\theta, \alpha_s, \lambda)$ can be expressed as:

$$L(\theta, \alpha_s, \lambda) = f(\theta, \alpha_s) + \lambda g(\theta, \alpha_s)^T \tag{26}$$

Here, λ is the vector of multipliers of equality constraint. If we denote $\theta^k = (\theta, \alpha_s)^T$, the Lagrangian function of the current problem can be written as

$L(\theta^k, \lambda^k) = f(\theta^k) + (\lambda^k)^T g(\theta^k)$. The quadratic programming (QP) sub-problem can be constructed by Taylor series approximation [41] as:

$$\begin{aligned} &\text{Minimize } \nabla L(\theta^k, \lambda^k)^T + \frac{1}{2} d^T H L(\theta^k, \lambda^k) d \text{ over } d \\ &= (\theta - \theta^k) \in \mathbb{R}^2 \text{ subject to } g(\theta^k) + \nabla g(\theta^k)^T d = 0 \end{aligned} \tag{27}$$

Here, λ^k is the Lagrangian multiplier associated with this QP. ∇ is the operator for partial derivative. H is the Hessian matrix of the Lagrangian function. Solving the Eq. (27) results in a solution vector $d = \theta - \theta^k$. The solution converges when the vector d is less than the relative tolerance of 0.0001 and when Karush–Kuhn–Tucker (KKT) criteria [41] are satisfied. In this problem, $\theta^k = (\theta, \alpha_s)^T$. The flow chart of the SQP algorithm to solve the nonlinear constraint problem is

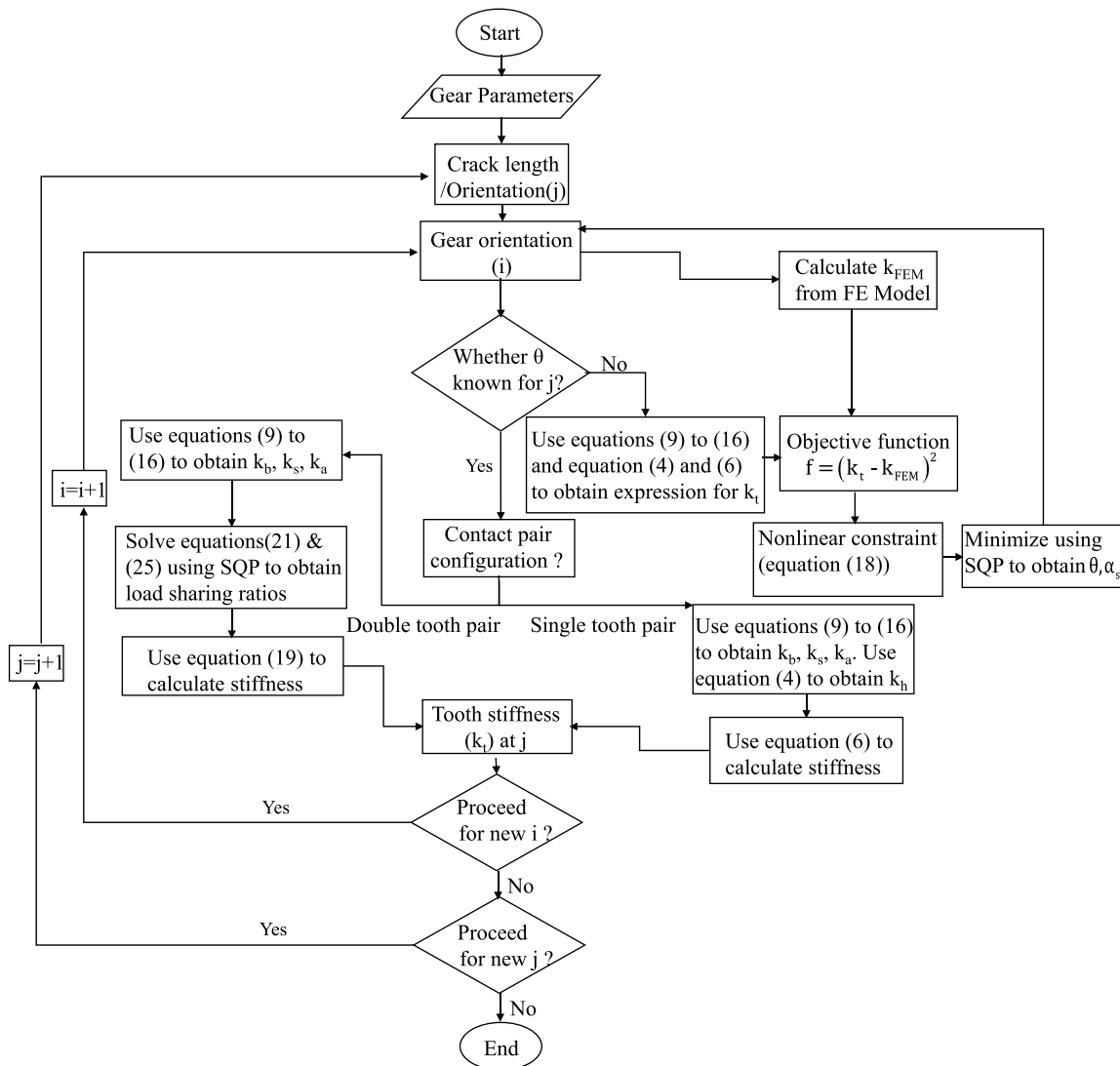


Fig. 7 Mesh stiffness calculation flow diagram using modified limiting line

Fig. 8 Mesh stiffness comparison between FEM and analytical methods (straight and parabolic limiting line) for crack levels. **a** 0 and 10%, **b** 40 and 50% for 20° crack angle

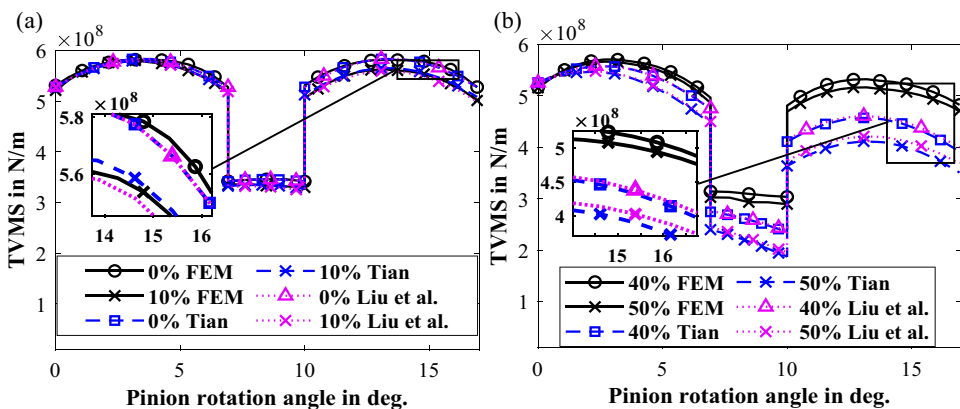


Table 2 Percentage difference using different analytical methods

Crack depth (%)	Difference (%) = $\frac{k_{fem} - k_{analytical}}{k_{fem}} \times 100$	
	Tian	Liu et al.
0	0.78	0.78
10	0.35	0.56
40	14.2	13.46
50	20.3	18.4

depicted in Fig. 5. A more detailed description of SQP can be found in reference [41].

Finite Element Method for Tooth Stiffness Evaluation

FE method has been used as an efficient and accurate tool for calculating time-varying mesh stiffness in spur gears. A three-dimensional model of spur gear with tooth crack, as shown in Fig. 6, is established here to calculate the tooth stiffness. The gear body is defined as rigid by assigning a

modulus of elasticity more than ten times that of the tooth material. For formation of a straight crack in ABAQUS, a partitioning strategy is used. The partitioning surface is defined as a seam so that nodes on crack surfaces do not interact with each other. Crack is then created, and crack front and crack propagation direction are selected along the seam. Contour integral method [42] is used to simulate the crack. Partitioning near the crack tip (Fig. 6b) is done to decrease the element size. Near the crack tip, wedge elements (Fig. 6b) are formed, whereas, outside the first contour, hexahedral C3D8 elements with swept meshing technique are used. Element sizes near the contact teeth (0.05 mm) and near crack front (0.01 mm) are chosen to be very small (Fig. 6b, c) in comparison with global element size of 1.2 mm.

A quasi-static approach is employed to determine the time-varying tooth stiffness. Gears are rotated gradually to simulate different mesh positions. Contacts between meshing tooth pairs are defined with a penalty approach for four tooth pairs shown in Fig. 6a. The driven gear is kept fixed, and the driving gear is subjected to a torque T (Fig. 6b). The gear parameters are listed in Table 1. The torsional deflection (θ) is obtained at the hub surface of the driven gear. The

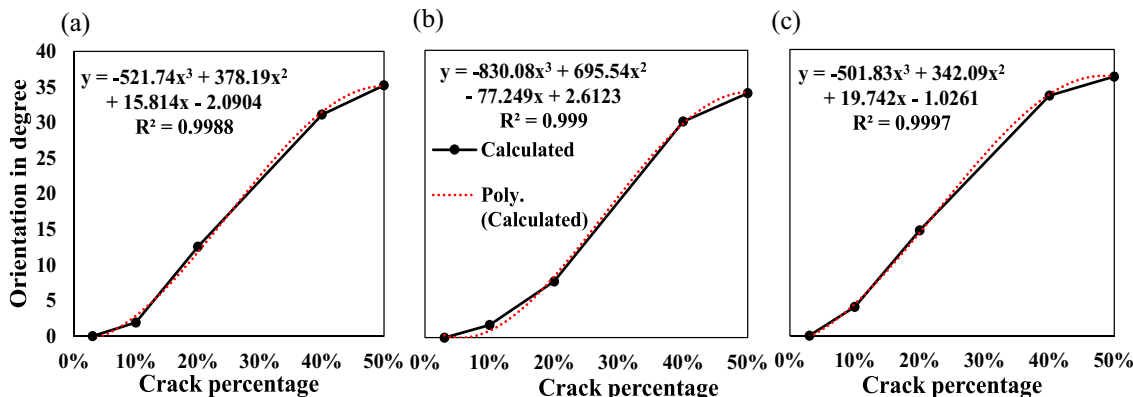
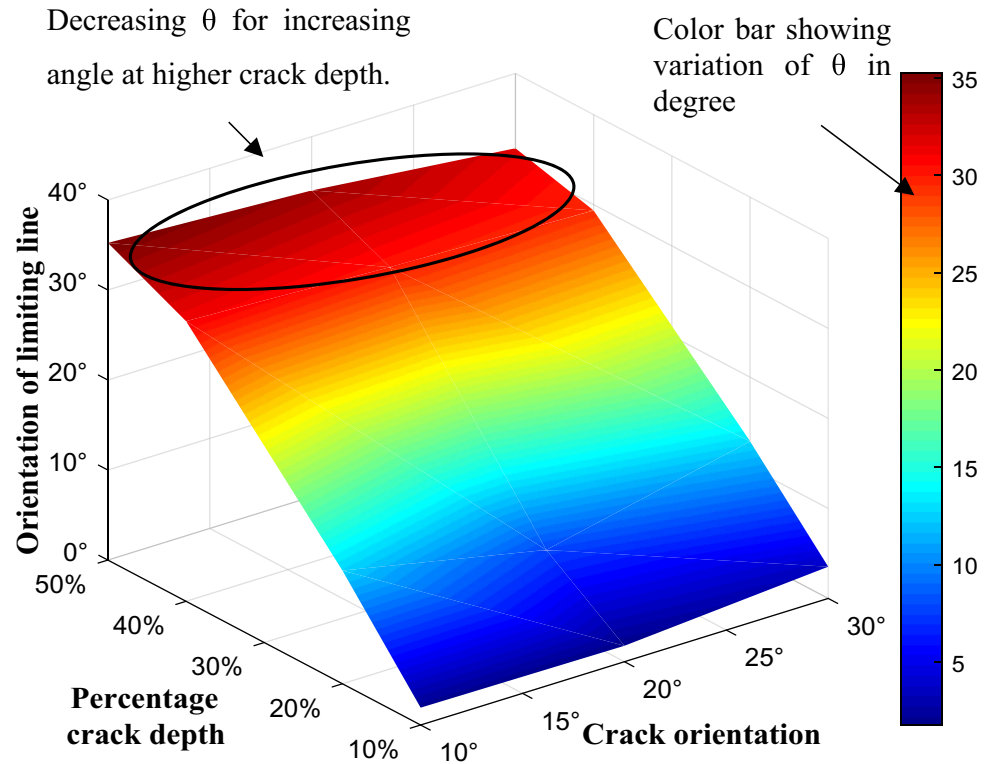


Fig. 9 Variation of orientation of modified limiting line with crack depth for crack angle. **a** 10°, **b** 20° and **c** 30°

Fig. 10 Variation of orientation (θ) of limiting line with crack depth percentage for increasing crack angle



rectilinear stiffness (k) can be calculated for various mesh positions using the equation given below [43]:

$$k = \frac{T}{r_b^2 \theta} \quad (28)$$

The time-varying tooth stiffness is calculated for various straight-line cracks of different depths and orientations.

Results and Discussion

Various gear parameters displayed in Table 1 are utilized to obtain the tooth stiffness using FE and analytical methods. For FE results, the methodology explained in "Proposed Tooth Stiffness Model for Cracked Case" is adopted. Gear flexibility is negated by assuming a large value of elastic modulus to the gear body. Cracks are assumed to propagate from the fillet region of the pinion tooth in straight paths (Fig. 1). Assuming a theoretical full length crack to be symmetrical [27] about the tooth midline, the crack depth (q) can be expressed as percentage with respect to the full length crack (q_f).

$$\text{Percentage crack length} = \frac{q}{q_f} \times 100$$

The crack length upto the tooth midline corresponds to a crack level of 50% irrespective of the crack orientation.

Results for five different health conditions of 0, 10, 20, 40 and 50% crack levels for three different crack orientations of 10°, 20° and 30° are obtained. FE simulations are carried out in ABAQUS CAE environment. For a particular health condition, as discussed above, gears are gradually rotated to obtain the torsional deflections, and they are further used in Eq. (28) to obtain the time-varying tooth stiffness. The analytical tooth stiffness for healthy gear is obtained using Tian's method [13] using Eqs. (1) to (6) given in "Traditional Time-Varying Tooth Stiffness Model for Cracked Tooth". To model the crack using existing methods, Tian's straight limiting line [13] and Liu et al.'s parabolic limiting curve [37, 38], as discussed in "Straight Limiting Line" and "Parabolic Limiting Line", respectively, are adopted. The tooth stiffness obtained using conventional limiting line methods is compared with FE results in "Comparison of Tooth Stiffness Using FEM and Traditional Method". The orientation of the modified limiting line is determined by solving the minimization problem as depicted in Eqs. (16) and (17) using the sequential quadratic programming algorithm explained in "Sequential Quadratic Programming". To thoroughly define the MLL for each crack configuration, only one FE simulation is performed at a particular gear meshing position. The same MLL is used to determine the mesh stiffness for other mesh positions for that crack configuration. Variation of the orientation of the new limiting line with respect to different crack levels is

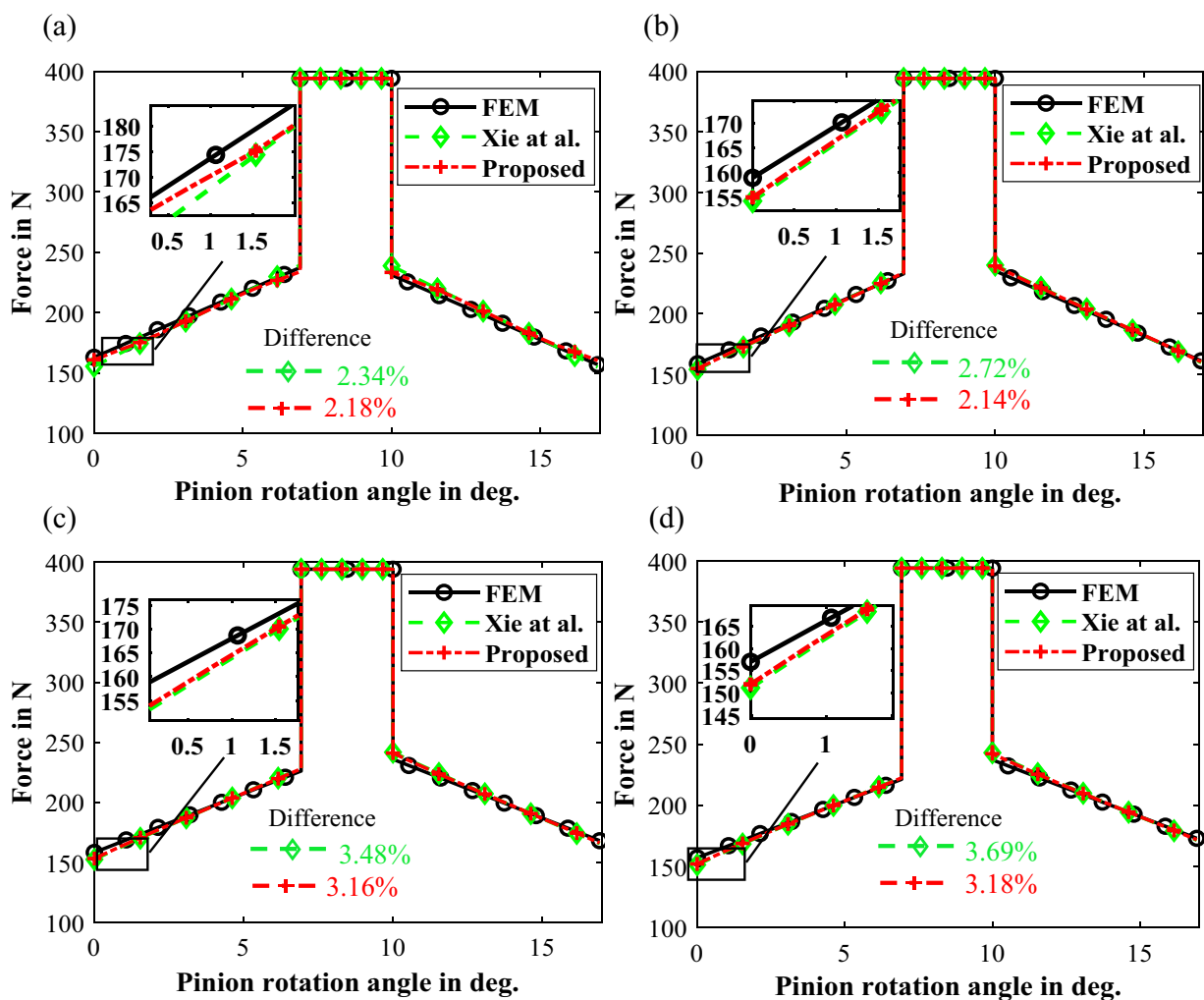


Fig. 11 Load sharing ratios during first cracked tooth pair for various crack levels. a 0% crack, b 20% crack, c 40% crack, d 50% crack

studied in "Determination of Orientation of the Proposed Limiting Line". The orientation of MLL is curve fitted for a few crack percentages. The polynomial fitted curve is later used to obtain orientation at other crack levels. Now, as the MLL is completely defined for a particular configuration, it is used to calculate the tooth stiffness during double tooth pair contact. The load sharing is first determined, and the proposed method is verified using FE method and the existing analytical method in "Verification of Load-Sharing Ratios During Double Tooth Pair Meshing". Finally, the time-varying tooth stiffness is obtained using the proposed method, and the results are compared with the FE and existing methods. A complete flow diagram for time-varying tooth stiffness calculation is given in Fig. 7.

Comparison of Tooth Stiffness Using FEM and Traditional Method

This section compares the time-varying tooth stiffness obtained with the results obtained by FE method with Tian's straight-line method [13] and Liu et al.'s parabolic curve [38].

Stiffness for healthy gear and three crack depths of 10, 40 and 50% for 20° crack angles are compared in Fig. 8. The percentage difference using various methods is shown in Table 2. The deviation of stiffness using the analytical and FE methods is minimal (less than 1%) for lower crack levels of 0 and 10%. However, with higher crack levels of 40 and 50%, deviations of stiffness using the traditional limiting line (straight) are 14 and 20%, respectively, as compared to FE method. Mohammed et al. [36] established similar results with higher crack levels. Liu et al.'s parabolic curve method only slightly improves the tooth stiffness at the higher crack levels compared to the straight limiting line. Therefore, for

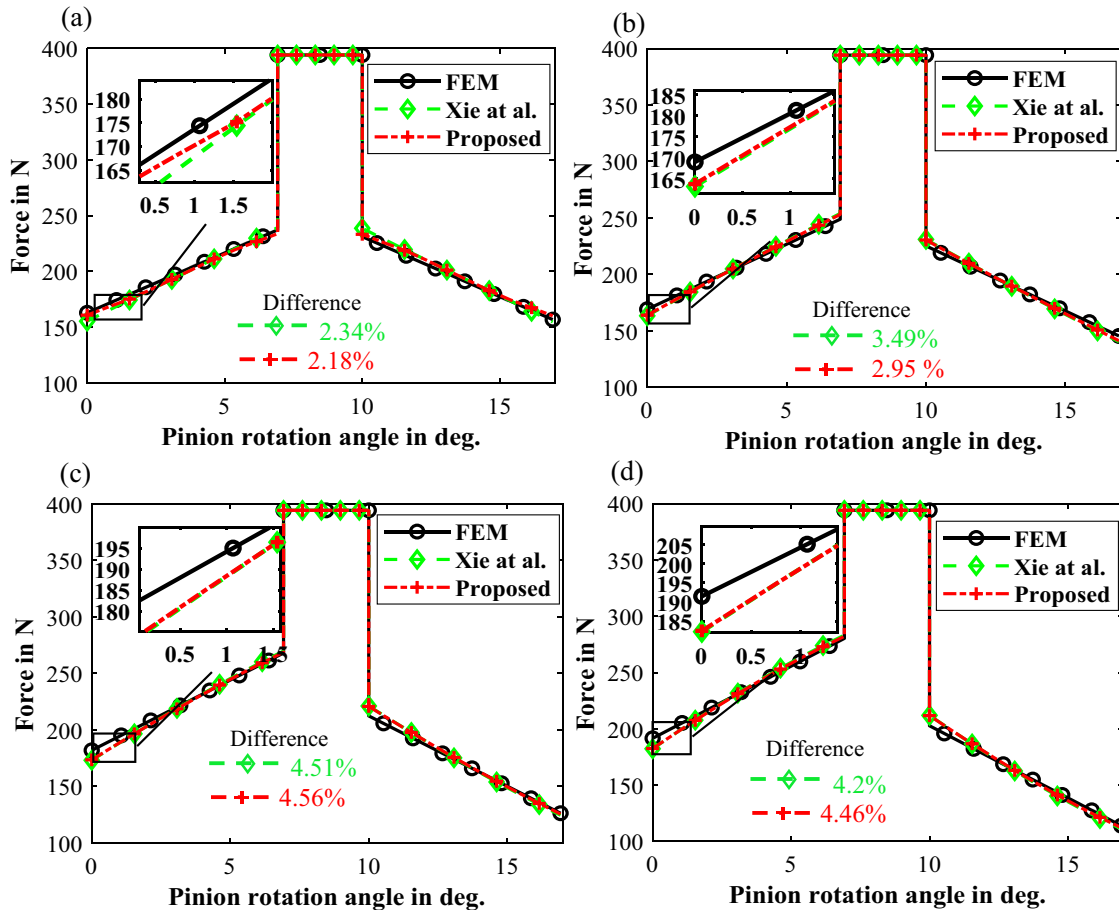


Fig. 12 Load sharing ratios during second cracked tooth pair for various crack levels. a 0% crack, b 20% crack, c 40% crack, d 50% crack

higher crack levels, both straight line and parabolic curve methods fail to calculate mesh stiffness accurately.

Determination of Orientation of the Proposed Limiting Line

As discussed in the last section, both the existing methods fail to model the crack accurately for higher crack levels; therefore, the modified limiting line (MLL) is incorporated to calculate the tooth stiffness of the gear pair. The modified limiting line is chosen as an oblique straight line (Fig. 3) in accordance with the discussions made for the cantilever problem in "Proposed Tooth Stiffness Model for Cracked Case". So, the orientation (θ) of the limiting line is of paramount importance, which is determined by the approach outlined in "Formulation of Minimization Problem for Determination of Orientation of Modified Limiting Line". The objective function formed in Eq. (17) with the nonlinear constraint (Eq. (18)) is solved using the sequential quadratic programming algorithm described in Fig. 5. The lower and upper bounds of θ are suitably selected. Figure 9a–c display the variation of θ against various crack depths for three

different crack angles of 10°, 20° and 30°, respectively. A polynomial fit is obtained with respect to crack depths. The R-squared values for each orientation are above 90%.

Moreover, the curve fitting equations displayed in Fig. 9 can be employed to obtain θ for various other crack levels for specific crack angles. Figure 10 shows the variation of orientation of limiting line with respect to crack percentage and orientations. The variation of blue to red color denotes an increase in limiting line angle. The orientation of MLL tends to increase with increase in crack percentage for all crack angles. The value of θ at lower crack levels tends to rise slightly with increasing crack angle, but as crack progresses, the rate of increase of θ with respect to crack orientation decreases. At 50% crack level, the value of θ decreases from 10° to 30° crack angle. The reason may be attributed to the increase in unloaded zone area towards the gear base due to the slant nature of crack path at higher crack angles. With lesser crack levels, the above phenomenon has little influence. As approximate equations for θ are available for various crack angles, the tooth stiffness can be obtained for any crack level between 0 to 50%. Now, the analytical method

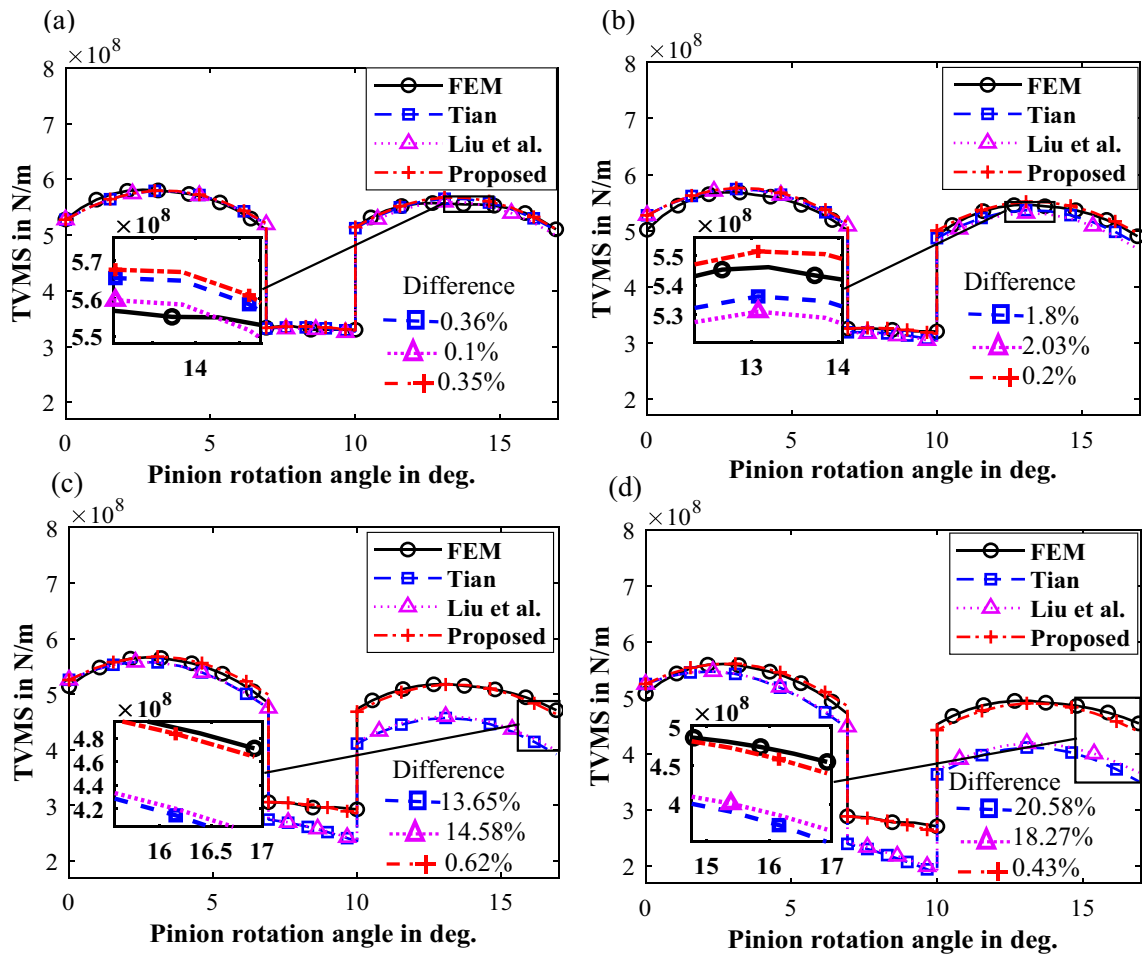


Fig. 13 Mesh stiffness comparison for different methods for crack angle of 10° for various crack levels of a 10%, b 20%, c 40% and d 50%

can be incorporated for various gear contact positions to calculate the time-varying tooth stiffness.

Verification of Load-Sharing Ratios During Double Tooth Pair Meshing

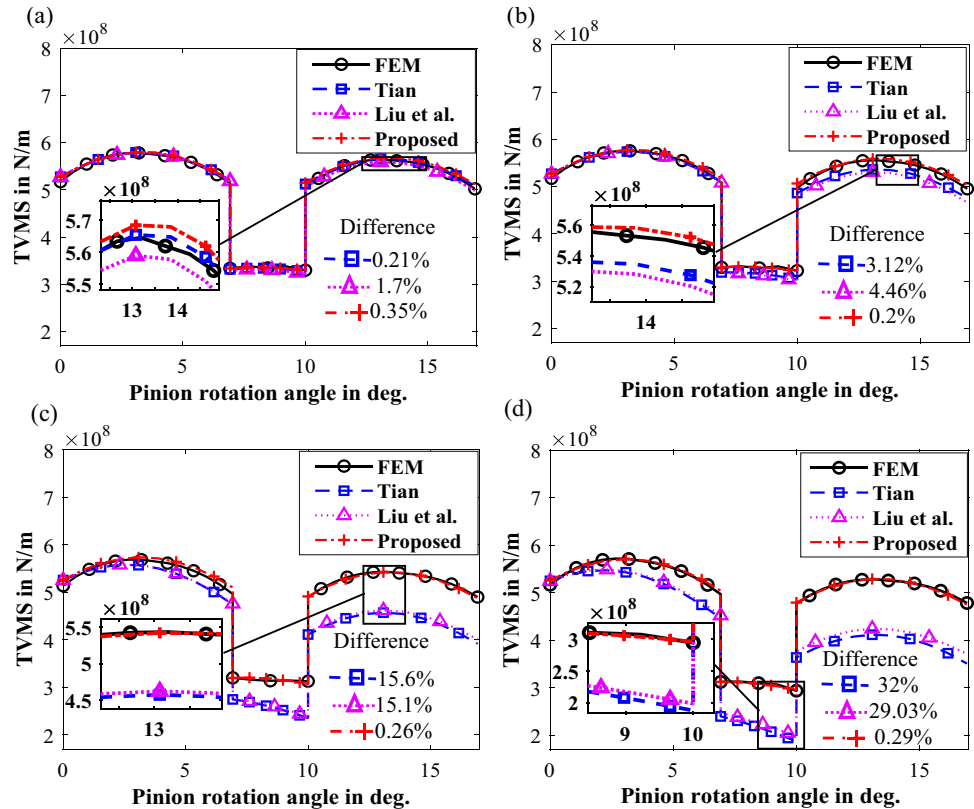
The accuracy of load sharing is important for accurate determination of tooth stiffness in gears. Contact ratio greater than one ensures that there is variation in tooth contact. In the present study, variation of tooth contact between single and double tooth pairs occurs due to a contact ratio of 1.693. The contact loads using FE method are obtained by requesting the contact forces for relevant surfaces in the history output request in ABAQUS CAE platform. The analytical contact loads are obtained using the method established by Xie et al. [17] and the proposed method that introduces the compatibility condition as outlined in "Tooth Stiffness During Double Tooth Pair Meshing". Results are compared in Figs. 11 and 12 for various crack depths for 10° crack

orientation. The pinion rotation angle is from tooth base to addendum.

The total contact load is approximately 394.14 N, corresponding to a 10 Nm torque. As the gears rotate, the cracked tooth moves from first tooth pair to second tooth pair position (Fig. 4). Figure 11 displays the shared loads during the position when crack is within the first tooth pair. The contact loads tend to decrease slightly for the first tooth, with a marginal increase in contact load for the second tooth. This is because the weakened tooth shares lesser load than the healthy tooth. This fact is also true for the second scenario when the crack is within the second tooth pair.

There is a reduction in shared load for the second tooth (cracked) and an increase for the first tooth, which is the healthy now. The discussions above for both scenarios establish the fact that the load-bearing capacity of a cracked tooth always reduces, and more load is shared by the healthy tooth. With an increase in crack depths from 0 to 50%, there is more reduction in shared load by the faulty tooth for both the cases (Figs. 11a–d, 12a–d). This also hints at the nature of mesh stiffness variation for the faulty and healthy tooth,

Fig. 14 Mesh stiffness comparison for different methods for crack angle of 30° for various crack levels of **a** 10%, **b** 20%, **c** 40%, **d** 50%



which will be discussed later. The proposed method for load-sharing calculation matches well with the existing method and FE method. However, the computational time is lesser for the proposed scheme (37.701483 s) compared with the existing method (58.211 s) in MATLAB platform. This is because the sequential quadratic programming searches for a local minimum, whereas the genetic algorithm used by Xie et al. [17] searches for a global minimum. The proposed scheme works well with the compatibility conditions.

Verification of Time-Varying Tooth Stiffness

In this section, the tooth stiffness obtained using the proposed method is verified using FE results. In addition, the proposed method is compared with the existing Tian's straight line [13] and Liu et al.'s [38] parabolic curve method. The tooth stiffness for traditional straight limiting line and parabolic limiting line are calculated as described in "Traditional Time-Varying Tooth Stiffness Model for Cracked Tooth". The orientation of the limiting line obtained for a particular gear meshing position during single tooth pair is used to obtain the tooth stiffness during other gear mating positions. Load sharing during double tooth pair contact is determined by solving Eqs. (23) and (25). Further, the mesh stiffness is obtained using Eqs. (19) and (21) described in "Tooth Stiffness During Double Tooth Pair Meshing". Figure 6 describes the complete workflow of time-varying tooth

stiffness evaluation. Figures 13 and 14 show the comparison of time-varying tooth stiffness using various methods for two different crack orientations of 10° and 30° , respectively. The stiffness reduction is more during the second tooth pair contact, which can be explained by the fact that the reduction of shared load is higher with higher pinion rotation angles (Figs. 11, 12).

The pinion rotation angle is calculated from base to tooth addendum. With 10% crack level Fig. 13a for 10° crack angle, the existing methods and the proposed method match well with the FE results. With higher crack percentages of 20, 40 and 50% in Fig. 13b–d, respectively, the deviation of the traditional straight line and parabolic curve method from the actual stiffness gradually increases.

Figure 14 depicts the mesh stiffness for 30° orientation crack. At higher crack levels around the 40–50% crack level (Fig. 14a, b), the parabolic curve approach deviates slightly less than the stiffness derived from the straight limiting line. At 10% crack depth, the outcomes are comparable to the stiffness obtained at 10° crack angle, and the deviations are lesser from the FE method. Nevertheless, the proposed technique demonstrates improved agreement in all crack situations considered above. Using a parabolic limiting line, as suggested by Liu et al., only marginally improves the stiffness calculation at higher crack levels.

Figure 15 depicts a comparison of the mesh stiffness for three crack angles for two distinct crack percentages. The

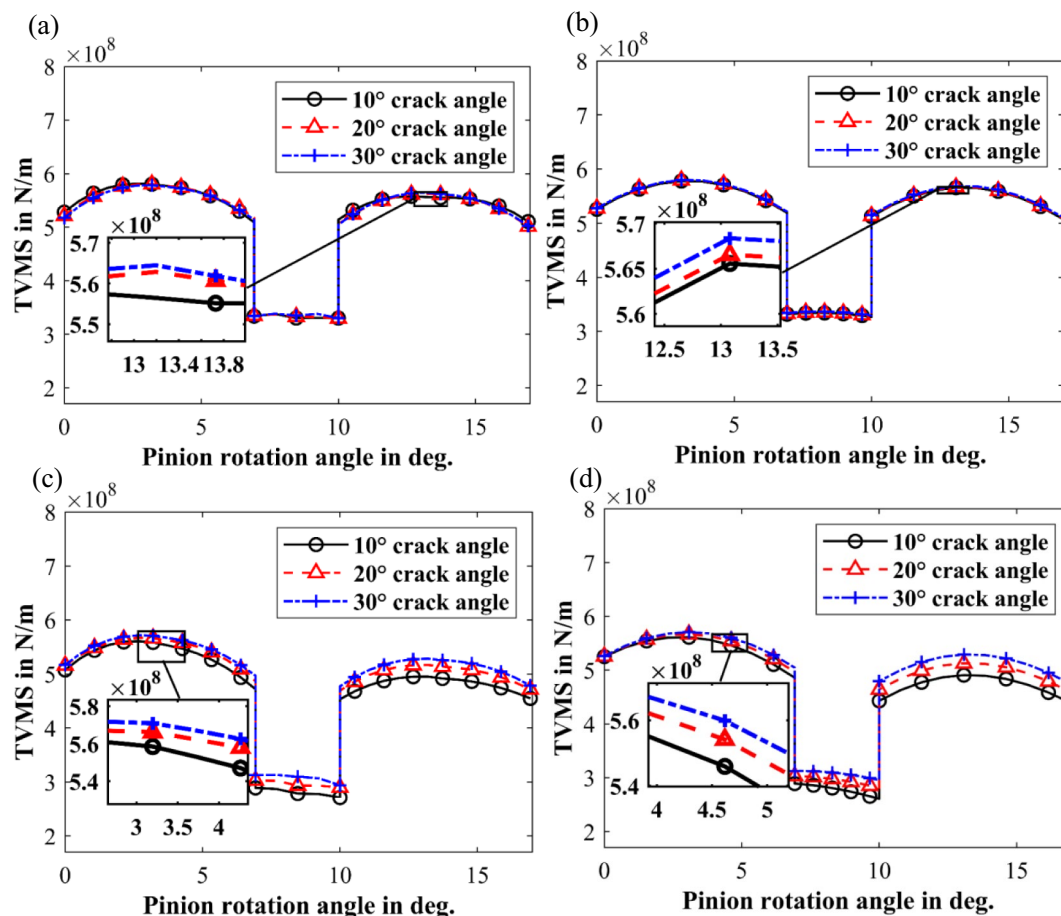


Fig. 15 Mesh stiffness comparison for different crack angles. **a** Proposed method (10% crack), **b** FE method (10% crack), **c** proposed method (50% crack), **d** FE method (50% crack)

proposed method (Fig. 15a, c) and the FE method (Fig. 15b, d) provide comparable results. The decrease in orientation of crack reduces the stiffness more at the 50% crack level compared to the 10% level. As the crack is steeper, the more is the tooth stiffness reduction. The rationale for the aforementioned phenomena is that a larger load-bearing zone occurs when the crack angle is greater, resulting in a decline in stiffness for the same crack percentage.

The quantification of deviation of various methods can be done by obtaining the errors. For all the three crack orientations and crack levels considered here, the maximum deviation occurs at the highest pinion rotation angle. The pinion rotation angle is taken from base of pinion to its tip. The maximum percentage error is calculated at the highest pinion rotational angle using the Eq. (28) below:

$$Error (\%) = \frac{TVMS_{FEM} - TVMS_{current\ method}}{TVMS_{FEM}} \times 100 \quad (29)$$

Figure 16a–c compare the greatest percentage error while utilizing the standard limiting line, the proposed limiting

line, and the parabolic limiting curve, respectively. The inaccuracy at greater crack levels is rather considerable for the straight-line method. For the parabolic curve approach, the inaccuracy decreases marginally when the proportion of cracks increases by over 15%. The greatest error for the proposed method is less than 5%

Dynamic Response

In the preceding section, the time-varying meshing stiffness of spur gear for various crack configurations was verified using FE method and discussed. The contribution of TVMS for different crack scenarios on dynamic response will be addressed. The 6 degrees of freedom lumped parameter model for single-stage spur gear is shown in Fig. 17, which includes the lateral and torsional degrees of freedom, respectively. As the responses in the x-directions are only transient responses without any external forces, the vibration in that direction is omitted from the present model.

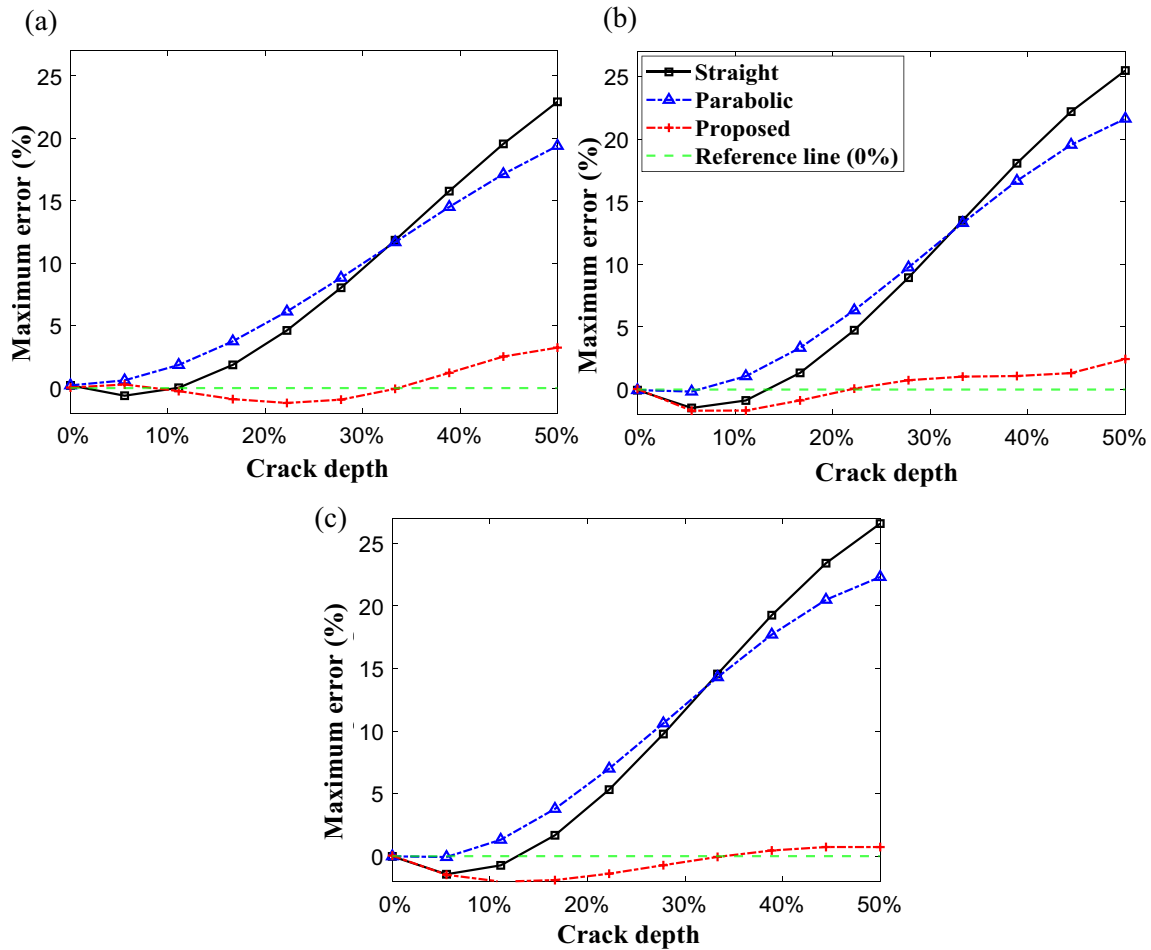


Fig. 16 Maximum percentage error for crack angles a 10°, b 20°, c 30°

The gear assembly model considers the meshing stiffness (k_t) and damping (c_t) of the gear pair along with torsional stiffness and damping of input (k_{cp} , c_{cp}) and output (k_{cg} , c_{cg}) shaft couplings. The bearings provide stiffness (k_{bp} , k_{bg}) and damping (c_{bp} , c_{bg}) along the line of action at pinion and gear locations. y_1 and y_2 represent the vibrations of pinion and gear in y-direction. m_1 and m_2 denote the masses of pinion and gear, respectively. I_m , I_2 , I_3 , I_b and θ_m , θ_1 , θ_2 , θ_b are the inertias and torsional deflections of motor, pinion, gear and the load, respectively.

The motion equations are derived [27] using Newton’s second law.

$$\begin{aligned}
 m_1 \frac{d^2 y_1}{dt^2} &= k_t(r_{b1}\theta_1 - r_{b2}\theta_2 - y_1 + y_2) \\
 &+ c_t \left(r_{b1} \frac{d\theta_1}{dt} - r_{b2} \frac{d\theta_2}{dt} - \frac{dy_1}{dt} + \frac{dy_2}{dt} \right) \\
 &- k_{bp}y_1 - c_{bp} \frac{dy_1}{dt}
 \end{aligned} \tag{30}$$

$$\begin{aligned}
 m_2 \ddot{y}_2 &= k_t(r_{b1}\theta_1 - r_{b2}\theta_2 - y_1 + y_2) \\
 &+ c_t(r_{b1}\dot{\theta}_1 - r_{b2}\dot{\theta}_2 - \dot{y}_1 + \dot{y}_2) \\
 &- k_{bg}y_2 - c_{bg}\dot{y}_2
 \end{aligned} \tag{31}$$

$$\begin{aligned}
 I_1 \ddot{\theta}_1 &= k_{cp}(\theta_m - \theta_1) - c_{cp}(\dot{\theta}_m - \dot{\theta}_1) \\
 &- r_{b1} \left[k_t(r_{b1}\theta_1 - r_{b2}\theta_2 - y_1 + y_2) \right. \\
 &\left. + c_t(r_{b1}\dot{\theta}_1 - r_{b2}\dot{\theta}_2 - \dot{y}_1 + \dot{y}_2) \right]
 \end{aligned} \tag{32}$$

$$\begin{aligned}
 I_2 \ddot{\theta}_2 &= -k_{cg}(\theta_2 - \theta_b) - c_{cg}(\dot{\theta}_2 - \dot{\theta}_b) \\
 &+ r_{b2} \left[k_t(r_{b1}\theta_1 - r_{b2}\theta_2 - y_1 + y_2) \right. \\
 &\left. + c_t(r_{b1}\dot{\theta}_1 - r_{b2}\dot{\theta}_2 - \dot{y}_1 + \dot{y}_2) \right]
 \end{aligned} \tag{33}$$

$$I_m \ddot{\theta}_m = T_m - k_{cp}(\theta_m - \theta_1) - c_{cp}(\dot{\theta}_m - \dot{\theta}_1) \tag{34}$$

$$I_b \ddot{\theta}_b = -T_b + k_{cg}(\theta_2 - \theta_b) + c_{cg}(\dot{\theta}_2 - \dot{\theta}_b) \tag{35}$$

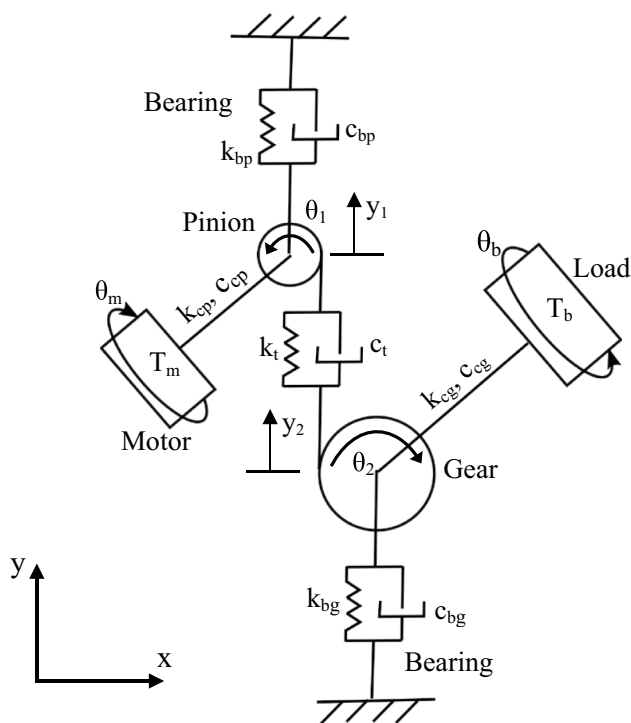


Fig. 17 Single stage gear box model [20]

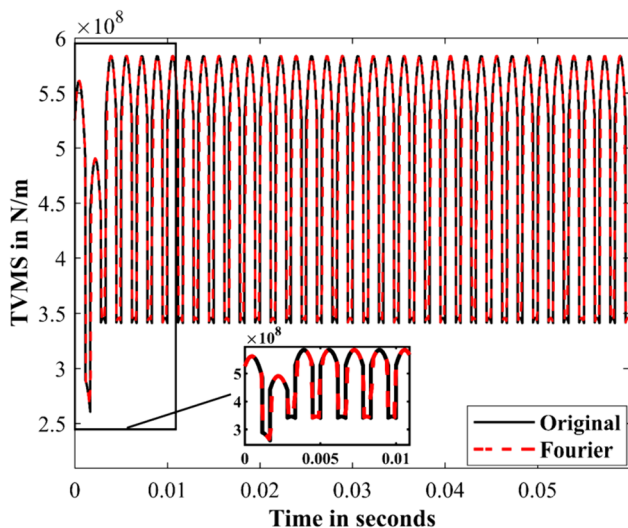


Fig. 18 Fourier series approximation of the original mesh stiffness using analytical method for 50% crack depth and 10° crack angle

The differential equations of motion for the single-stage gear system require that the mesh stiffness is provided in continuous equation form. The Fourier series is used to fit the TVMS obtained. Fast Fourier Transform is used to obtain the frequency components with the corresponding amplitudes. Further, they are used to generate the mesh stiffness curve. Figure 18 shows the comparison of the Fourier fitted curve with the original

Table 3 Parameters of gear-rotor system for dynamic simulation

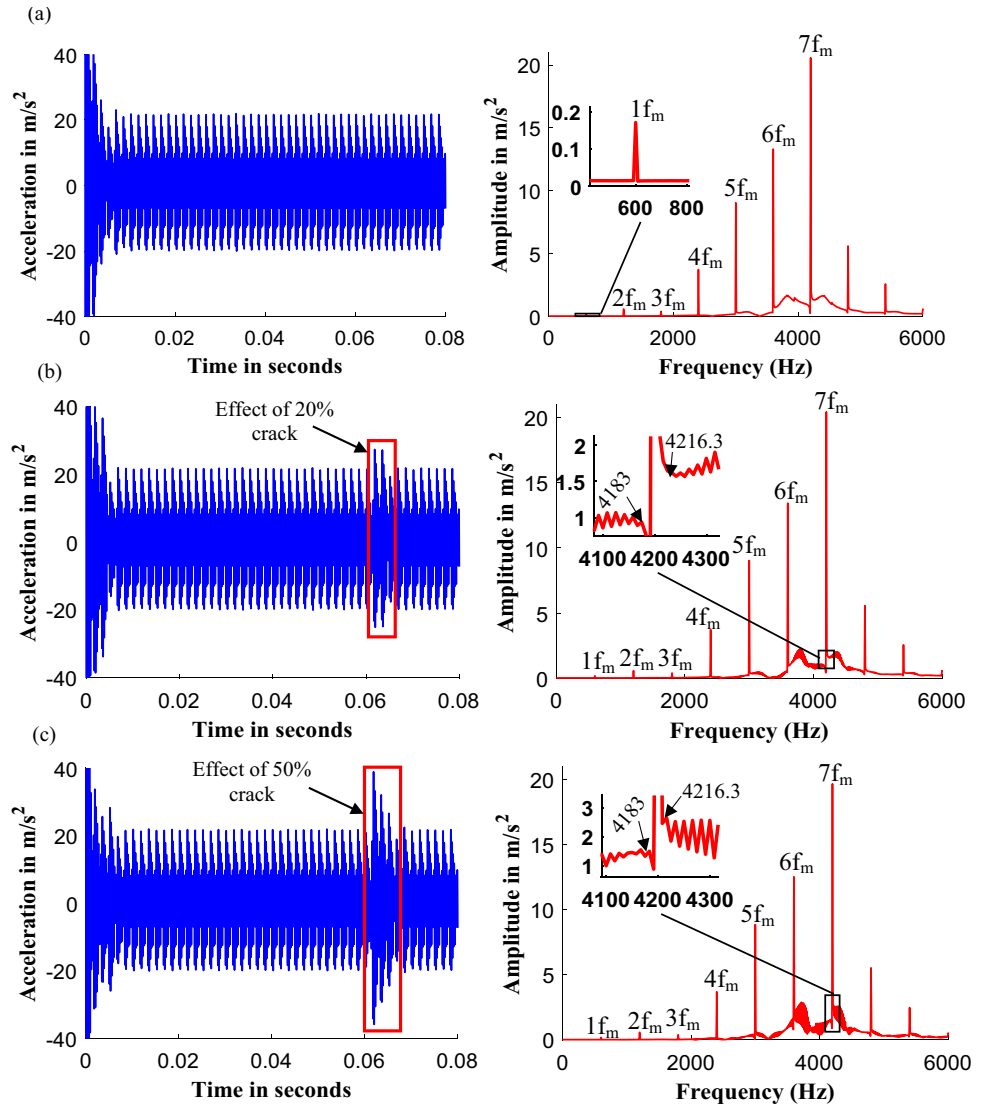
Gear assembly property	Symbol	Value
Mass of pinion/gear	m_1/m_2	0.2327 kg
Mass moment of inertia of motor	I_m	0.0021 kg m ²
Mass moment of inertia of load	I_b	0.0105 kg m ²
Mass moment of inertia of pinion/gear	I_1/I_2	9.6454×10^{-5} kg m ²
Input motor torque	T_m	11.9 Nm
Braking torque	T_b	11.9 Nm
Radial stiffness of bearing	k_b	6.56×10^7 N/m
Radial damping of bearing	c_b	1.8×10^5 Ns/m
Torsional stiffness of shaft coupling	k_c	4.4×10^4 Nm/rad
Torsional damping of shaft coupling	c_c	5×10^5 Nms/rad
Input frequency	f	16.67 Hz
Gear meshing frequency	f_m	600 Hz

curve for crack configuration of 50% depth and 10° crack angle. For the pinion having 36 teeth, the mesh stiffness is shown here for one complete revolution of pinion at 1000 RPM speed. A good fit is obtained with around 2401 number of frequency values.

The time-varying mesh stiffness damping (c_t) is taken proportional to k_t and the proportionality constant is calculated as 2.2447×10^{-6} s for a damping ratio of 0.07 using the method prescribed in Ref. [13]. The parameters given in Table 3 and suitable initial conditions are substituted into the differential equation for rotational speed of 1000 RPM. The differential equations of motion (Eq. (30) to (35)) are solved by a variable step, variable order solver based on numerical differentiation, popularly known as ODE 15 s in MATLAB and dynamic response of the gear pair during healthy and faulty states are obtained.

Figure 19 shows both the time domain and frequency domain responses of the acceleration signal in vertical direction (y-direction in Fig. 17) at the pinion location for various fault states. The healthy response is shown in Fig. 19a. The frequency spectrum shows the peaks at gear meshing frequency ($f_m = 600$ Hz) and its harmonics. The maximum amplitude occurs at 7th harmonic. The advent of crack induces sidebands around the gear meshing frequency and its harmonics at frequencies $Nf_m \pm nf$. Where f is the rotational frequency, which is around 16.67 Hz for an input speed of 1000 RPM, N represents the harmonics of gear mesh frequency, and n is a whole number. This transforms as peaks at the rotational period in the time domain signal. At 20% crack level (Fig. 19b), sidebands are less prominent at the 7th harmonics as compared to 50% crack level (Fig. 19c).

Fig. 19 Dynamic response at pinion in time and frequency domain for various crack levels. **a** Healthy, **b** 20%, **c** 50% at 1000 RPM input speed



Also, the peak amplitude in time domain signal is higher for 50% crack level as compared to 20% crack level.

In Fig. 19, the sidebands are prominent at higher crack levels only. So, to get a more significant influence of the crack on sidebands, the frequency spectrums are obtained for various input speeds. Figure 20 shows the 3d plot for the frequency spectrum for various input speed ranging from 800 to 1500 RPM. The family of sidebands is more significant at 1100 RPM, 1200 RPM and 1300 RPM. However, the peak acceleration shifts towards lower harmonics at higher speeds. Apart from the frequency domain characteristics, the time domain statistical indicators play a vital role in fault diagnosis using vibration monitoring. In the succeeding section, the influence of crack on such indicators is discussed.

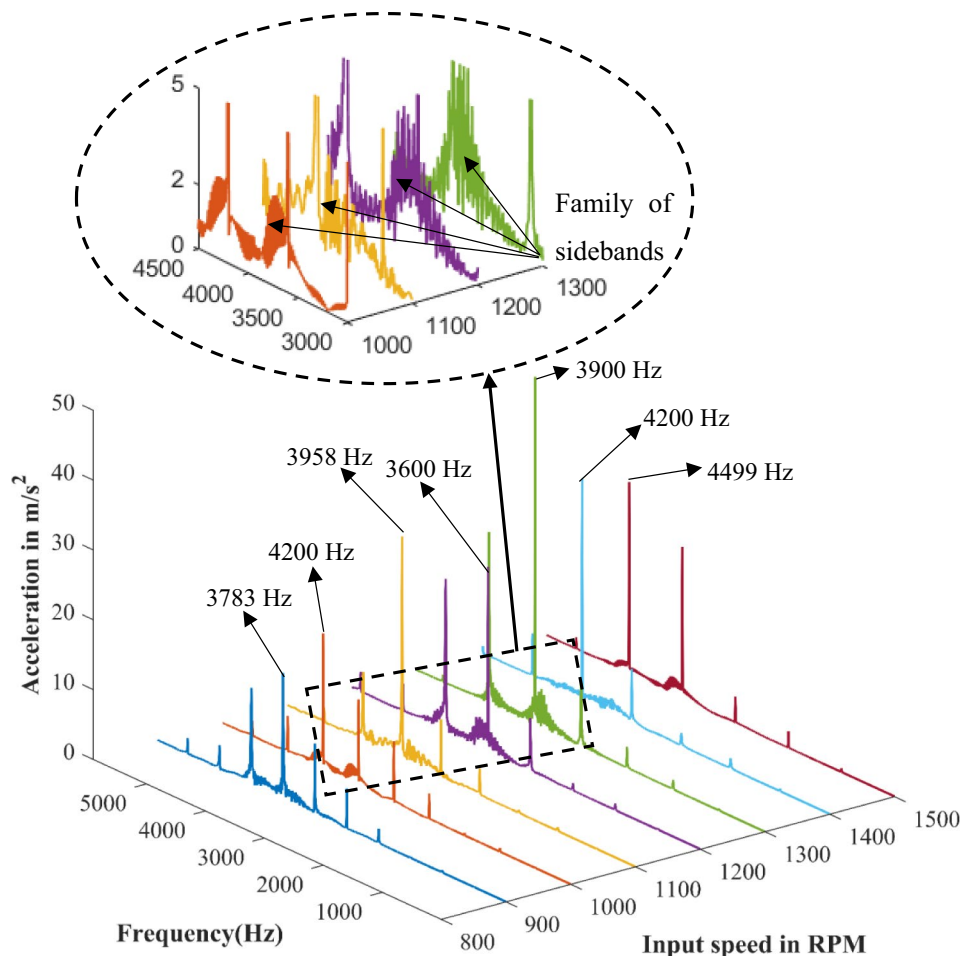
Influence of Crack on Time Domain Statistical Indicators

In this section, various time-domain statistical parameters like rms, skewness, crest factor and kurtosis are obtained from the residual signal. The time domain indicators [26] are briefly explained by Eqs. (36), (37), (38), (39). In the equations below, N is the number of data points, x_i is the amplitude at the i^{th} point of the signal, and \bar{x} is the mean value of the signal.

$$RMS = \sqrt{\frac{1}{N} \sum_{i=1}^N (x_i - \bar{x})^2} \tag{36}$$

$$Skewness = \frac{\sum_{i=1}^N (x_i - \bar{x})}{(N - 1)\sigma^3} \tag{37}$$

Fig. 20 Frequency spectrum for 50% crack level for different input speed



$$Kurtosis = \frac{(1/N) \sum_{i=1}^N (x_i - \bar{x})^4}{\left[(1/N) \sum_{i=1}^N (x_i - \bar{x})^2 \right]^2} \tag{38}$$

$$Crest\ factor = \frac{\max(x_i)}{RMS} \tag{39}$$

To obtain the statistical indicators, two methods have been utilized, which are explained below.

Method 1 Each of the statistical indicators can be obtained for healthy and fault cases. Percentage difference is calculated using the formula below (Eq. (40)).

$$Difference\ (\%) = \frac{I_f - I_h}{I_h} \times 100 \tag{40}$$

Herein, I_f is the indicator of faulty response, I_h represent the indicator for the healthy response.

Method 2 The residual signal, representing the difference between faulty and healthy cases, contains information about the severity of the crack. Figure 21 depicts the residual signal obtained for 10° crack angle for various

crack levels. The peaks tend to increase as the crack level increases from Fig. 21a–d. In this method, the statistical indicators are obtained for the residual signals around the maximum amplitude zone.

Figure 22a displays the variation of the statistical indicators for different crack levels using method 1. The skewness is overall the better performer among other indicators. The crest factor is the second-best parameter for detection of the fault. Both kurtosis and RMS perform badly using method 1.

The variation of statistical parameters using method 2 is shown in Fig. 22b. RMS is the best indicator using method 2. All the other parameters fare very badly. The above two methods require that a healthy signal is available beforehand.

Conclusions

In this work, a modified limiting line is established to calculate the gear mesh stiffness that can be utilized more generally for lower and higher crack levels. Gear body flexibility is not considered here for simplicity and to avoid any error due to gear body stiffness calculations. A minimization

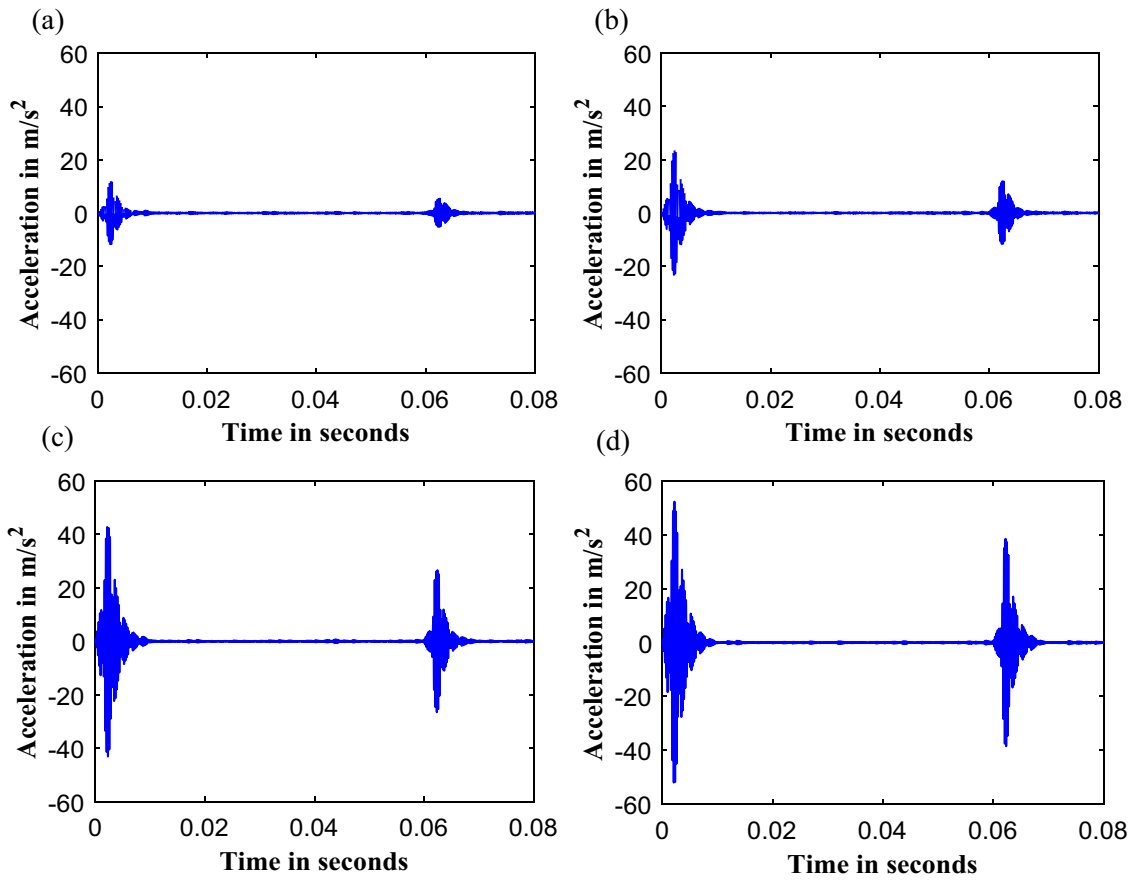


Fig. 21 Residual response for various crack levels. a 10%, b 20%, c 40%, d 50%

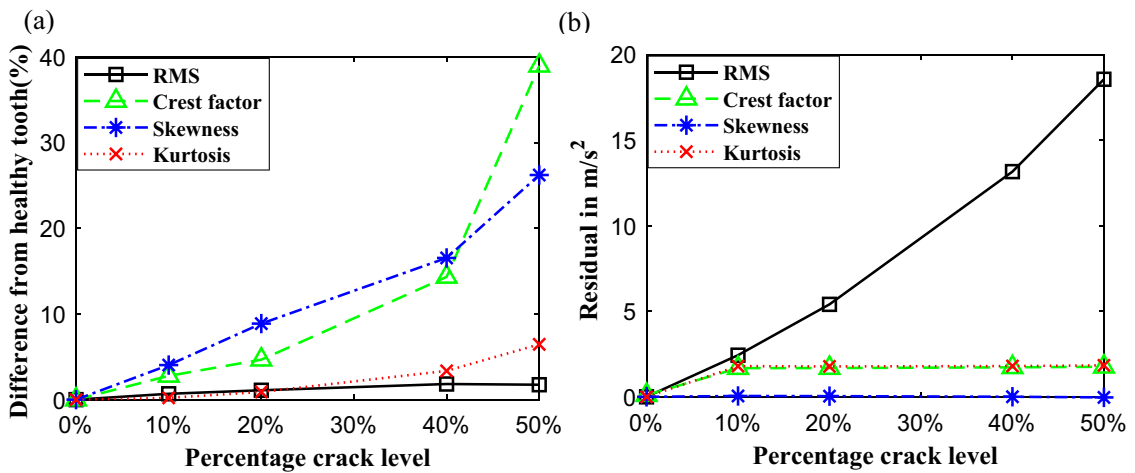


Fig. 22 Statistical indicators variation using a method 1, b method 2

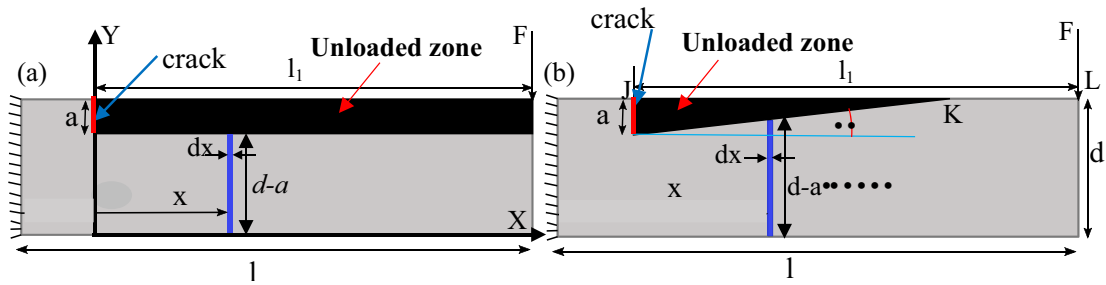


Fig. 23 Cantilever beam with a traditional and b proposed limiting line

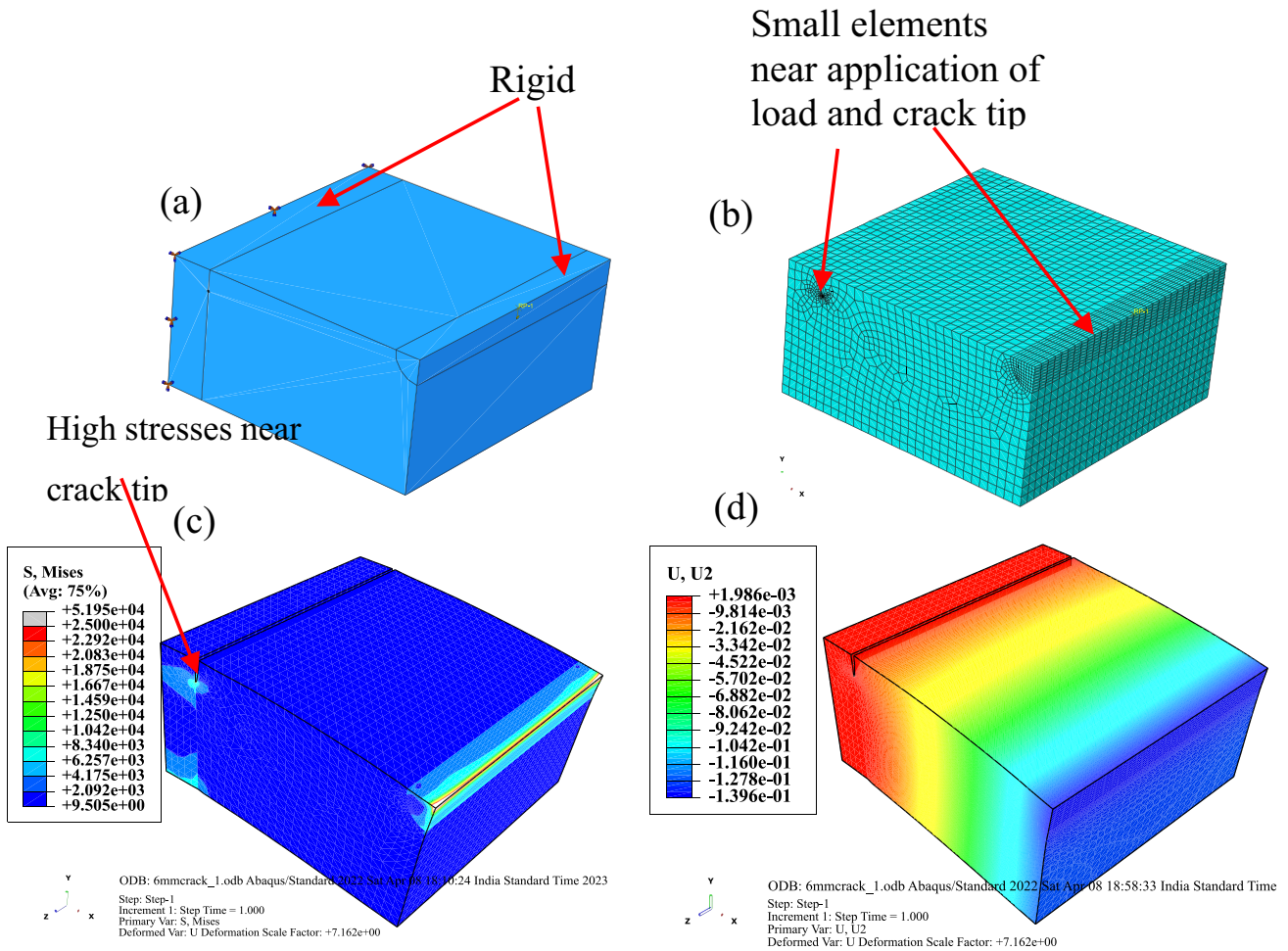


Fig. 24 a Boundary condition, b FE meshing, c Von Mises stress, d deflection

problem is formulated by comparing the analytical mesh stiffness of cracked spur gear with the finite element method at a particular gear orientation. The orientation of the new limiting line is obtained by solving the minimization problem using the sequential quadratic programming algorithm. Next, the orientation is used to obtain the mesh stiffness at other gear meshing points. Moreover, a compatibility condition is proposed in "Tooth Stiffness During Double Tooth

Pair Meshing" in accordance with the existing minimization of potential energy approach for load sharing determination. SQP is used to solve the above optimization problem. Mesh stiffness is obtained for various crack levels and angles. The proposed method is compared with FE method, and other existing methods and results are analyzed for various crack configurations. Also, to have an overview of the contribution of crack on vibration, the dynamic responses are obtained,

and frequency and time domain analyses have been performed. The following conclusions can be drawn:

- In practice, the mesh stiffness of a cracked gear is calculated using a straight limiting line and a parabolic curve. The straight line generates significant inaccuracy at greater crack depths. In addition, the current research demonstrates that the shape of parabolic curve used in earlier studies does not significantly enhance the mesh stiffness estimations. The proposed model can more precisely predict the gear pair's mesh stiffness.
- The present semi-analytical method uses results from FE method to calculate the orientation of the new limiting line. However, it differs from the traditional FE methods by considering only one gear meshing position during single tooth pair contact for the calculation of orientation of limiting line. The same orientation is used to further to calculate mesh stiffness at other meshing points. So, number of FE simulations is lesser.
- The accuracy of orientation of the new limiting line depends upon the accuracy of FE method at a particular gear contact position for various crack configurations. With increase in crack length, the orientation of the oblique line tends to increase, which shows that most of the unloaded zone is closer to the crack.
- The crack angle also affects the orientation of the modified limiting line; as the angle of the crack grows, so does the orientation of the line. However, the orientation tends to decrease marginally as the fracture angle increases with increasing crack depth.
- The proposed scheme for calculating load-sharing ratios during double tooth pair meshing validates well with the FE method and the existing method with an improvement in computational time.
- The proposed mesh stiffness calculation method is verified using the FE method and shows significant improvements compared to traditional and parabolic limiting lines. The maximum percentage error of mesh stiffness calculation using the proposed method is less than 5% for crack levels up to 50%. In addition, as gear body and tooth stiffness calculations are separate, the present method can be applied in conjunction with the gear body flexibility.
- The dynamic responses show modulation of healthy signal when crack is introduced. Family of sidebands can be seen with increasing crack levels in frequency domain. Various statistical indicators are obtained using two methods for various crack levels. One method shows the skewness and crest factor as the best indicators, whereas the other method, considering the residual signal, shows RMS as the best indicator.

Appendix A Example of a Cantilever Beam for Establishing the Modified Limiting Line

The existing tooth stiffness evaluation methods consider the gear tooth as a cantilever beam fixed at its base circle. In this section, a cantilever whose dimensions are comparable to those of a gear tooth is used to illustrate the limitations of the traditional limiting line, and a modified limiting line is introduced to address the flaw. A vertical load is applied at the free end (Fig. 23a) so that total potential energy is sum of only bending energy (U_b) and shearing energy (U_s) given by Eq. (41).

$$\begin{aligned} \text{Bending energy } U_b &= \frac{F^2}{2k_b} = \int_0^l \frac{M_x^2 dx}{2EI_x}, \\ \text{Shearing energy } U_s &= \frac{F^2}{2k_s} = \int_0^l \frac{1.2F_x^2 dx}{2GA_x} \end{aligned} \quad (41)$$

Therefore, the expression for equivalent stiffness (k) can be written as follows:

$$\frac{1}{k} = \frac{1}{k_b} + \frac{1}{k_s} \quad (42)$$

Dimensions of the cantilever beam are chosen similarly to the dimensions of a gear tooth. Length (l) = 10 mm, width (b) = 10 mm, depth (d) = 5 mm, length (l_1) = 8.5 mm (Fig. 23a).

A vertical crack is assumed to propagate in the beam. The portion between fixed end and crack position in Fig. 23a, b is assumed to be rigid. The dark strips in Fig. 23a, b represent the traditional and modified dead zones, respectively. So, any crack in the beam modifies moment of inertia I_x and area A_x at a distance x from Y-axis shown in Fig. 23a, b and expressions for I_x and A_x are given below in Eqs. (43), (44) and (45) for different cases case.

$$\text{For healthy beam } I_x = \frac{bd^3}{12} \text{ and } A_x = bd \quad (43)$$

For cracked beam using traditional limiting line

$$I'_x = \frac{b(d-a)^3}{12} \text{ and } A'_x = b(d-a) \quad (44)$$

For cracked beam using the modified limiting line,

$$I_x'' = \left\{ \begin{array}{l} \frac{b(d-a+x \tan \theta)^3}{12} \text{ from J to K} \\ \frac{bd^3}{12} \text{ from K to L} \end{array} \right\} \text{ and} \quad (45)$$

$$A_x'' = \left\{ \begin{array}{l} b(d-a+x \tan \theta) \text{ from J to K} \\ bd \text{ from K to L} \end{array} \right\}$$

Here, a is the crack length, θ is the orientation of the modified limiting line. Using the traditional limiting line, expressions for equivalent stiffness can be directly obtained by replacing I_x'' and A_x'' in place of I_x and A_x in Eqs. (9) and (10). The proposed limiting line requires that θ to be determined, which is calculated by equating the strain energy release (ΔU) (Eq. (46)) with the FE method.

$$\Delta U = \int_0^{a \cot \theta} \frac{F^2(l-x)^2}{2E} \left(\frac{12}{b(d-a+x \tan \theta)^3} - \frac{12}{bd^3} \right) dx$$

$$+ \int_0^{a \cot \theta} \frac{F^2}{2G} \left(\frac{1}{b(d-a+x \tan \theta)} - \frac{1}{bd} \right) dx \quad (46)$$

For different crack depths, the cantilever is simulated in the ABAQUS CAE platform to obtain the strain energy release using the J-integral approach for different crack depths. A 3-D model is established where the free end is subjected to a force of 10 N. To avoid flexibility due to local deformation, the location near the point of application of load (Fig. 24a) is assigned with modulus elasticity, which is twenty times the modulus of elasticity of the material. The load is applied at the reference point that is coupled to the free end of the beam. Hexahedral elements of type C3D8 are used for meshing. Small elements are used near the application of load (Fig. 24b). Wedge elements with a median axis are selected at the crack front. Figure 24c, d show the stresses in MPa and deflections (δ) in mm. The stiffness is calculated using the formula $k = F/\delta$. The stiffness is obtained for crack levels.

Funding No funding was received to assist with the preparation of this manuscript.

Declarations

Conflict of interest The authors have no relevant financial or non-financial interests to disclose. The authors have no competing interests to declare that are relevant to the content of this article. All authors certify that they have no affiliations with or involvement in any organization or entity with any financial interest or non-financial interest in the subject matter or materials discussed in this manuscript. The authors have no financial or proprietary interests in any material discussed in this article.

References

1. Yesilyurt I, Gu F, Ball AD (2003) Gear tooth stiffness reduction measurement using modal analysis and its use in wear fault severity assessment of spur gears. *NDT E Int* 36:357–372
2. Munro RG, Palmer D, Morrish L (2001) An experimental method to measure gear tooth stiffness. *Instrumentation* 215:793–803
3. Pandya Y, Parey A (2013) Experimental investigation of spur gear tooth mesh stiffness in the presence of crack using photoelasticity technique. *Eng Fail Anal* 34:488–500
4. Raghuvanshi NK, Parey A (2015) Mesh stiffness measurement of cracked spur gear by photoelasticity technique. *Meas J Int Meas Confed* 73:439–452
5. Raghuvanshi NK, Parey A (2016) Experimental measurement of gear mesh stiffness of cracked spur gear by strain gauge technique. *Meas J Int Meas Confed* 86:266–275
6. Mahapatra S, Shrivastava A, Sahoo B et al (2023) Estimation of torque variation due to torsional vibration in a rotating system using a Kalman filter-based approach. *J Vib Eng Technol* 11:1939–1950
7. Wang J (2003) Numerical and experimental analysis of spur gears in mesh. Ph.D Thesis, Curtin University, Department of Mechanical Engineering
8. Arafa MH, Megahed MM (1999) Evaluation of spur gear mesh compliance using the finite element method. *Proc Inst Mech Eng Part C J Mech Eng* 213:569–579
9. Cooley CG, Liu C, Dai X et al (2016) Gear tooth mesh stiffness: a comparison of calculation approaches. *Mech Mach Theory* 105:540–553
10. Liang X, Zhang H, Liu L et al (2016) The influence of tooth pitting on the mesh stiffness of a pair of external spur gears. *Mech Mach Theory* 106:1–15
11. Wang J, Howard I (2005) Finite element analysis of high contact ratio spur gears in mesh. *J Tribol* 127:469–483
12. Yang DCH, Lin JY (1987) Hertzian damping, tooth friction and bending elasticity in gear impact dynamics. *J Mech Des Trans ASME* 109:189–196
13. Tian X (2004) Dynamic simulation for system response of gearbox including localized gear faults. Master's thesis, University of Alberta, Canada
14. Chen Z, Shao Y (2013) Mesh stiffness calculation of a spur gear pair with tooth profile modification and tooth root crack. *Mech Mach Theory* 62:63–74
15. Sainsot P, Velex P, Duverger O (2004) Contribution of gear body to tooth deflections—a new bidimensional analytical formula. *J Mech Des Trans ASME* 126:748–752
16. Muskhelishvili N (1977) Some basic problems of the mathematical theory of elasticity, 2nd edn. Noordhoff International Publishing, Leyden. <https://doi.org/10.1007/978-94-017-3034-1> (**Epub ahead of print 1977**)
17. Xie C, Hua L, Han X et al (2018) Analytical formulas for gear body-induced tooth deflections of spur gears considering structure coupling effect. *Int J Mech Sci* 148:174–190
18. Ambarisha VK, Parker RG (2007) Nonlinear dynamics of planetary gears using analytical and finite element models. *J Sound Vib* 302:577–595
19. Ma H, Pang X, Feng R et al (2015) Improved time-varying mesh stiffness model of cracked spur gears. *Eng Fail Anal* 55:271–287
20. Dai H, Long X, Chen F et al (2021) An improved analytical model for gear mesh stiffness calculation. *Mech Mach Theory* 159:104262
21. Ma H, Zeng J, Feng R et al (2016) An improved analytical method for mesh stiffness calculation of spur gears with tip relief. *Mech Mach Theory* 98:64–80
22. Lewicki DG Gear crack propagation path studies guidelines for ultra-safe design. NASA/TM-2001-211073

23. Lewicki DG, Ballarini R (1997) Effect of rim thickness on gear crack propagation path. *J Mech Des Trans ASME* 119:88–95
24. Lewicki DG, Ballarini R (1998) Gear crack propagation investigations. *Tribotest* 5:157–172
25. Verma JG, Kumar S, Kankar PK (2018) Crack growth modeling in spur gear tooth and its effect on mesh stiffness using extended finite element method. *Eng Fail Anal* 94:109–120
26. Zouari S, Maatar M, Fakhfakh T et al (2007) Three-dimensional analyses by finite element method of a spur gear: effect of cracks in the teeth foot on the mesh stiffness. *J Fail Anal Prev* 7:475–481
27. Wu S, Zuo MJ, Parey A (2008) Simulation of spur gear dynamics and estimation of fault growth. *J Sound Vib* 317:608–624
28. Mohammed OD, Rantatalo M, Aidanpää JO et al (2013) Vibration signal analysis for gear fault diagnosis with various crack progression scenarios. *Mech Syst Signal Process* 41:176–195
29. Chaari F, Baccar W, Abbes MS et al (2008) Effect of spalling or tooth breakage on gearmesh stiffness and dynamic response of a one-stage spur gear transmission. *Eur J Mech A/Solids* 27:691–705
30. Zhou X, Shao Y, Lei Y et al (2012) Time-varying meshing stiffness calculation and vibration analysis for a 16DOF dynamic model with linear crack growth in a pinion. *J Vib Acoust Trans ASME* 134:1–11
31. Chen Z, Shao Y (2011) Dynamic simulation of spur gear with tooth root crack propagating along tooth width and crack depth. *Eng Fail Anal* 18:2149–2164
32. Yang L, Wang L, Shao Y et al (2021) A new calculation method for tooth fillet foundation stiffness of cracked spur gears. *Eng Fail Anal* 121:105173
33. Huang K, Yi Y, Xiong Y et al (2020) Nonlinear dynamics analysis of high contact ratio gears system with multiple clearances. *J Braz Soc Mech Sci Eng* 42:1–16
34. Namboothiri NV, Marimuthu P (2022) Fracture characteristics of asymmetric high contact ratio spur gear based on strain energy release rate. *Eng Fail Anal* 134:106038
35. Mohammed OD (2023) Crack detection of a modified high contact ratio gear. *Eng Fail Anal* 152:107493
36. Mohammed OD, Rantatalo M, Aidanpää JO (2013) Improving mesh stiffness calculation of cracked gears for the purpose of vibration-based fault analysis. *Eng Fail Anal* 34:235–251
37. Cui L, Zhai H, Zhang F (2015) Research on the meshing stiffness and vibration response of cracked gears based on the universal equation of gear profile. *Mech Mach Theory* 94:80–95
38. Liu Y, Shi Z, Liu X et al (2022) Mesh stiffness model for spur gear with opening crack considering deflection. *Eng Fail Anal* 139:106518
39. Yang Y, Tang J, Hu N et al (2023) Research on the time-varying mesh stiffness method and dynamic analysis of cracked spur gear system considering the crack position. *J Sound Vib* 548:117505
40. Nocedal J, Wright SJ (2006) *Numerical optimization*, 2nd edn. Springer, Evanston
41. Rao SS (2009) *Engineering optimization—theory and practice*, 4th edn. Wiley, New York
42. Anderson TLA (1994) *Fracture mechanics—fundamentals and applications*, 4th edn. CRC Press, New York
43. Howard I, Jia S, Wang J (2001) The dynamic modelling of a spur gear in mesh including friction and a crack. *Mech Syst Signal Process* 15:831–853

Publisher's Note Springer Nature remains neutral with regard to jurisdictional claims in published maps and institutional affiliations.

Springer Nature or its licensor (e.g. a society or other partner) holds exclusive rights to this article under a publishing agreement with the author(s) or other rightsholder(s); author self-archiving of the accepted manuscript version of this article is solely governed by the terms of such publishing agreement and applicable law.